ERAD inhibition, detecting properly folded MHC class I by W6/32 antibody,[12,29] but we cannot exclude the possibility that eeyarestatin I induces UPR through an accumulation of incorrectly folded proteins. On the other hand, monensin has been reported to neutralize acidic intracellular compartments such as the *trans*-Golgi apparatus *via* its ionophore activity, and to inhibit *medial*- to *trans*-Golgi protein transport.[30–32] Hence, we cannot exclude the possibility that inhibition of *medial*- to *trans*-Golgi protein transport by monensin abrogates the entire protein transport system, including transport from the ER to the Golgi apparatus, resulting in an accumulation of correctly folded proteins in the ER. This possibility was confirmed by our observation that another polyether K^+/H^+ ionophore, nigericin, which disrupts Golgi function similarly to monensin,[30,33] also upregulated GRP78 protein expression (Fig. S2).

What remains unclear is the reason the compounds in cluster A and cluster B induced different expression patterns of the UPR target genes (Fig. 5). As shown in Fig. 5, the compounds in cluster A and cluster B comparatively highly upregulated the genes belonging to cluster I, GRP78, ERdj4, EDEM1, $p58^{IPK}$, and GRP94, and cluster II, GADD34, CHOP, PDI, and ATF4, respectively. Since the expression of a UPR target gene is transcriptionally regulated by the activation of three ER stress sensors (ATF6, IRE1, and PERK), it is possible that each of these stress sensors has distinct sensitivity to compounds belonging to cluster A and cluster B, resulting in higher expression of the genes in cluster I and cluster II respectively. Indeed, it has been reported that GRP94 and GRP78 are regulated by ATF6,[34,35] ERdj4 is regulated by IRE1,[36–38] and EDEM1 and $p58^{IPK}$ are regulated by both IRE1 and ATF6.[34,37,38] On the other hand, among the genes to be classified in cluster II, the expression of GADD34 and CHOP was reported to be regulated by PERK.[15,39,40] Furthermore, since a previous study found that the PDI gene has a sequence resembling the ATF-binding site in its promoter region,[41] the expression of PDI, a gene in cluster II, might also be mediated by ATF4 and its upstream ER stress sensor, PERK. Thus, it is likely that ATF6 and IRE1 are sensitive to compounds in cluster A in comparison with PERK, and that PERK is sensitive to compounds in cluster B as compared to ATF6 and IRE1. On the other hand, among the compounds in the same cluster, little difference in the expression patterns of the UPR target genes was observed. For instance, tunicamycin highly upregulated $p58^{IPK}$ and GRP94 as compared to thapsigargin, 2-deoxyglucose, and DTT. 2-Deoxyglucose and DTT highly upregulated GRP78 and ERdj4 as compared to thapsigargin and tunicamycin. In order to compare these differences more clearly, we are developing a new detection system to monitor the activation kinetics of the three ER stress sensors.

In summary, we classified the expression patterns of nine UPR target genes induced by seven UPR-inducing compounds into two clusters by hierarchal clustering analysis. Our results suggest the existence of at least two types of UPR target gene expression profiles, which might be dependent on the mode of action of the compounds. To our knowledge, although there have been many reports on the regulatory mechanism of UPR target gene expression using UPR-inducing compounds, they have failed to address the question whether the difference in mode of action of the UPR-inducing compounds influences the expression patterns of UPR target genes. This study is a first approach this question by statistical analysis, and provides the information that the expression patterns of UPR target genes are indeed different among the compounds. We hypothesize that the sensitivity of the three ER stress sensors depends on the folding status of the accumulated proteins in the ER, which results in the different expression patterns of the UPR target genes. Further study is needed to elucidate our hypothesis that the folding status of the accumulated proteins affects the activation of ER stress sensors, the expression of UPR target genes, and consequent responses, such as protein refolding, protein degradation, and apoptosis.

Acknowledgments

This work is supported by Grants-in-Aid for Scientific Research (KAKENHI grant no. 23510283, to E.T.) from Ministry of Education, Culture, Sports, Science and Technology (MEXT), Japan. S.S. was a research assistant in the Global COE Program for Human Metabolomic Systems Biology.

References

1) Ron D and Walter P, *Nat. Rev. Mol. Cell Biol.*, **8**, 519–529 (2007).
2) Zhao L and Ackerman SL, *Curr. Opin. Cell Biol.*, **18**, 444–452 (2006).
3) Olden K, Pratt RM, Jaworski C, and Yamada KM, *Proc. Natl. Acad. Sci. USA*, **76**, 791–795 (1979).
4) Takatsuki A, Kohno K, and Tamura G, *Agric. Biol. Chem.*, **39**, 2089–2091 (1975).
5) Price BD, Mannheim-Rodman LA, and Calderwood SK, *J. Cell. Physiol.*, **152**, 545–552 (1992).
6) Thastrup O, Cullen PJ, Drøbak BK, Hanley MR, and Dawson AP, *Proc. Natl. Acad. Sci. USA*, **87**, 2466–2470 (1990).
7) Cleland WW, *Biochemistry*, **3**, 480–482 (1964).
8) Halleck MM, Holbrook NJ, Skinner J, Liu H, and Stevens JL, *Cell Stress Chaperones*, **2**, 31–40 (1997).
9) Citterio C, Vichi A, Pacheco-Rodriguez G, Aponte AM, Moss J, and Vaughan M, *Proc. Natl. Acad. Sci. USA*, **105**, 2877–2882 (2008).
10) Liu E and Ou J, *J. Biol. Chem.*, **267**, 7128–7133 (1992).
11) Datema R and Schwarz RT, *Biochem. J.*, **184**, 113–123 (1979).
12) Fiebiger E, Hirsch C, Vyas JM, Gordon E, Ploegh HL, and Tortorella D, *Mol. Biol. Cell*, **15**, 1635–1646 (2004).
13) Wang Q, Mora-Jensen H, Weniger MA, Perez-Galan P, Wolford C, Hai T, Ron D, Chen W, Trenkle W, Wiestner A, and Ye Y, *Proc. Natl. Acad. Sci. USA*, **106**, 2200–2205 (2009).
14) Watowich SS and Morimoto RI, *Mol. Cell. Biol.*, **8**, 393–405 (1988).
15) Novoa I, Zeng H, Harding HP, and Ron D, *J. Cell Biol.*, **153**, 1011–1022 (2001).
16) Yan W, Frank CL, Korth MJ, Sopher BL, Novoa I, Ron D, and Katze MG, *Proc. Natl. Acad. Sci. USA*, **99**, 15920–15925 (2002).
17) Sasazawa Y, Futamura Y, Tashiro E, and Imoto M, *Cancer Sci.*, **100**, 1460–1467 (2009).
18) Tashiro E, Hironiwa N, Kitagawa M, Futamura Y, Suzuki S, Nishio M, and Imoto M, *J. Antibiot.*, **60**, 547–553 (2007).
19) Dean R and Dixon W, *Anal. Chem.*, **23**, 636–638 (1951).
20) Kawamura T, Matsubara K, Otaka H, Tashiro E, Shindo K, Yanagita RC, Irie K, and Imoto M, *Bioorg. Med. Chem.*, **19**, 4377–4385 (2011).
21) Haney ME Jr and Hoehn MM, *Antimicrob. Agents Chemother.*, **7**, 349–352 (1967).

22) Harding HP, Zhang Y, and Ron D, *Nature*, **397**, 271–274 (1999).
23) Di Jeso B, Ulianich L, Pacifico F, Leonardi A, Vito P, Consiglio E, Formisano S, and Arvan P, *Biochem. J.*, **370**, 449–458 (2003).
24) Kurtoglu M, Gao N, Shang J, Maher JC, Lehrman MA, Wangpaichitr M, Savaraj N, Lane AN, and Lampidis TJ, *Mol. Cancer Ther.*, **6**, 3049–3058 (2007).
25) Schwarz RT, Schmidt MF, and Datema R, *Biochem. Soc. Trans.*, **7**, 322–326 (1979).
26) Kaufman RJ, *Genes Dev.*, **13**, 1211–1233 (1999).
27) Lefrancois L and Lyles DS, *Virology*, **121**, 157–167 (1982).
28) Preston AM, Gurisik E, Bartley C, Laybutt DR, and Biden TJ, *Diabetologia*, **52**, 2369–2373 (2009).
29) Parham P, Barnstable CJ, and Bodmer WF, *J. Immunol.*, **123**, 342–349 (1979).
30) Dinter A and Berger EG, *Histochem. Cell Biol.*, **109**, 571–590 (1998).
31) Griffiths G, Quinn P, and Warren G, *J. Cell Biol.*, **96**, 835–850 (1983).
32) Mollenhauer HH, Morre DJ, and Rowe LD, *Biochim. Biophys. Acta*, **1031**, 225–246 (1990).
33) Craig S and Goodchild DJ, *Protoplasma*, **122**, 91–97 (1984).
34) Yamamoto K, Sato T, Matsui T, Sato M, Okada T, Yoshida H, Harada A, and Mori K, *Dev. Cell*, **13**, 365–376 (2007).
35) Yoshida H, Haze K, Yanagi H, Yura T, and Mori K, *J. Biol. Chem.*, **273**, 33741–33749 (1998).
36) Kanemoto S, Kondo S, Ogata M, Murakami T, Urano F, and Imaizumi K, *Biochem. Biophys. Res. Commun.*, **331**, 1146–1153 (2005).
37) Lee AH, Iwakoshi NN, and Glimcher LH, *Mol. Cell. Biol.*, **23**, 7448–7459 (2003).
38) Yoshida H, Matsui T, Hosokawa N, Kaufman RJ, Nagata K, and Mori K, *Dev. Cell*, **4**, 265–271 (2003).
39) Harding HP, Novoa I, Zhang Y, Zeng H, Wek R, Schapira M, and Ron D, *Mol. Cell*, **6**, 1099–1108 (2000).
40) Ma Y and Hendershot LM, *J. Biol. Chem.*, **278**, 34864–34873 (2003).
41) Tasanen K, Oikarinen J, Kivirikko KI, and Pihlajaniemi T, *J. Biol. Chem.*, **267**, 11513–11519 (1992).

The Journal of Antibiotics (2013) 66, 165–170

www.nature.com/ja

ORIGINAL ARTICLE

Novel derivatives of aclacinomycin A block cancer cell migration through inhibition of farnesyl transferase

Shigeyuki Magi[1,3], Tetsuo Shitara[2,3], Yasushi Takemoto[1], Masato Sawada[1], Mitsuhiro Kitagawa[1], Etsu Tashiro[1], Yoshikazu Takahashi[2] and Masaya Imoto[1]

In the course of screening for an inhibitor of farnesyl transferase (FTase), we identified two compounds, *N*-benzyl-aclacinomycin A (ACM) and *N*-allyl-ACM, which are new derivatives of ACM. *N*-benzyl-ACM and *N*-allyl-ACM inhibited FTase activity with IC_{50} values of 0.86 and 2.93 μM, respectively. Not only ACM but also C-10 epimers of each ACM derivative failed to inhibit FTase. The inhibition of FTase by *N*-benzyl-ACM and *N*-allyl-ACM seems to be specific, because these two compounds did not inhibit geranylgeranyltransferase or geranylgeranyl pyrophosphate (GGPP) synthase up to 100 μM. In cultured A431 cells, *N*-benzyl-ACM and *N*-allyl-ACM also blocked both the membrane localization of H-Ras and activation of the H-Ras-dependent PI3K/Akt pathway. In addition, they inhibited epidermal growth factor (EGF)-induced migration of A431 cells. Thus, *N*-benzyl-ACM and *N*-allyl-ACM inhibited EGF-induced migration of A431 cells by inhibiting the farnesylation of H-Ras and subsequent H-Ras-dependent activation of the PI3K/Akt pathway.
The Journal of Antibiotics (2013) **66,** 165–170; doi:10.1038/ja.2012.108; published online 30 January 2013

Keywords: aclacinomycin A; cancer cell migration; farnesyl transferase

INTRODUCTION

Cell migration is not only a central feature of a range of physiological processes, but also a crucial event in the spread of cancer and, consequently, the metastatic process.[1] Ras protein, a guanine nucleotide (GTP) binding protein, has an important role in signal transduction and regulation of cell migration.[2,3] A series of post-translational modifications are essential for the cell membrane association of Ras protein. One key modification is farnesylation of Ras by farnesyl transferase (FTase) on the C-terminus cystein residue of the CAAX motif.[4] Previously, we screened for inhibitors of cancer cell migration and obtained moverastin A and B, new members of the cylindrol family, from *Aspergillus* sp. F7720.[5] Furthermore, we found that moverastin A and B inhibited FTase, and demonstrated that moverastins inhibited the migration of tumor cells by inhibiting the farnesylation of H-Ras. However, the inhibitory activity of moverastins for FTase was rather modest (IC_{50} value of 14.7 μM). Thus we started screening of potent inhibitors of FTase as part of the project in Screening Committee of Anticancer Drugs (SCADS). In this study, we found new inhibitors of FTase, *N*-benzyl-aclacinomycin A (ACM) and *N*-allyl-ACM, which are chemically synthesized derivatives of ACM (aclarubicin) and described the antimigrative effect of these compounds.

MATERIALS AND METHODS

General experimental procedures

Centrifugal partition chromatography was performed using a centrifugal partition chromatograph-L.L.N. (Model-NMF, 250 ml cell; Sanki Engineering, Tokyo, Japan). HRMS were recorded on an Accu TOF-T100LC (JEOL, Tokyo, Japan) mass spectrometer. ^{1}H-NMR and ^{13}C-NMR data were measured on a JEOL ECX-600 spectrometer. Chemical shifts for proton are reported in p.p.m. downfield from tetramethylsilane. For ^{13}C NMR, chemical shifts were reported in the scale relative to NMR solvent ($CDCl_3$: 77.0 p.p.m.) as an internal reference. Optical rotations were measured with a P-1030 polarimeter (JASCO, Tokyo, Japan). IR spectra were recorded on a FT/IR-4100 Fourier transform IR spectrometer (JASCO).

Preparation of *N*-benzyl-ACM

ACM hydrochloride (255.9 mg, 0.301 mM) in dry dimethylformamide (5.2 ml) was treated with benzyl bromide (0.108 ml, 3.0 equiv.) in the presence of diisopropylethylamine (0.315 ml, 6.0 equiv.) at room temperature for 19 h. After removal of the solvent, the residue was dissolved in $CHCl_3$, washed with H_2O and then continuously with aqueous Na_2SO_4. The $CHCl_3$ layer was dried over Na_2SO_4 and evaporated. The oily residue was washed with hexane-diethyl ether (4:1) three times and the remaining residue (crude material 1) (328.4 mg) was purified by centrifugal partition chromatography ($CHCl_3$: CH_3OH: H_2O = 5:6:4, ascending mode), to give mixtures containing

[1]Faculty of Science and Technology, Department of Biosciences and Informatics, Keio University, Yokohama, Japan and [2]Institute of Microbial Chemistry (BIKAKEN), Tokyo, Japan
Correspondence: Professor M Imoto, Faculty of Science and Technology, Department of Biosciences and Informatics, Keio University, Yokohama 223-8522, Japan.
E-mail: imoto@bio.keio.ac.jp
or Professor Y Takahashi, Institute of Microbial Chemistry (BIKAKEN), 3-14-23 Kamiosaki, Shinagawa-ku, Tokyo 141-0021, Japan.
E-mail: Takahashiy@bikaken.or.jp
[3]These authors contributed equally to this work.
Received 25 September 2012; revised 1 November 2012; accepted 9 November 2012; published online 30 January 2013

N-benzyl-ACM (151.28 mg). The portion (118.6 mg) of obtained crude materials was passed through a Dowex 1 × 2 (chloride form, CH_3OH: H_2O = 1:4), and finally purified by silica gel column chromatography ($CHCl_3$: CH_3OH: H_2O = 10:1:0.1), to give pure *N*-benzyl-ACM (71.4 mg, yield 32%) as an orange powder.

HRMS (ESI$^+$ mode): *m/z* 902.39627 (observed), *m/z* 902.39575 (calcd. for $C_{49}H_{60}NO_{15}^+$); ^{1}H-NMR of rhodosamine and D-ring moieties (chemical shift in p.p.m., splitting pattern, *J* in Hz) in $CDCl_3$: H-7 (5.18, d, 5.5), H-8a (2.20, d, 15.0), H-8b (2.61, dd, 5.5 and 15.0), 9-OH (4.57, br s), H-10 (4.12, s), H-13a (1.69, dq, 7.5 and 15.0), H-13b (1.79, dq, 7.5 and 15.0), H-14 (1.15, t, 7.5), -COOMe (3.69, s), H-1′ (5.81, br d, 2.0), H-2′a (overlapping at around 2.1 p.p.m.), H-2′b (overlapping at around 2.4 p.p.m.), H-3′ (5.13, br d, 14.0), H-4′ (4.45, br s), H-5′ (overlapping at around 4.55p.p.m.), H-6′ (1.38, d, 7.0). *Optical rotation*: $[\alpha]_D^{26}$ +23 (*c* 0.1, $CHCl_3$) NMR table of *N*-benzyl-ACM is presented in Table 1.

Preparation of *N*-allyl-ACM

ACM hydrochloride (259.2 mg, 0.305 mM) in dry dimethylformamide (5.2 ml) was treated with allyl iodide (0.042 ml, 1.5 equiv.) in the presence of diisopropylethylamine (0.16 ml, 3.0 equiv.) at room temperature for 24 h. The reagents allyl iodide (0.028 ml, 1.0 equiv.) and diisopropylethylamine (0.053 ml, 1.0 equiv.) were added and the reaction mixtures were maintained for a further 7 h. After removal of the solvent, the residue was dissolved in $CHCl_3$, washed with H_2O and then continuously with aqueous Na_2SO_4. The $CHCl_3$ layer was dried over Na_2SO_4 and evaporated. The oily residue was washed with hexane-diethyl ether (4:1) three times and the remaining residue (crude material **2**) (302.8 mg) was purified by centrifugal partition chromatography ($CHCl_3$: CH_3OH: H_2O = 5:6:4, ascending mode), to give mixtures containing *N*-allyl-ACM (108.2 mg). The crude materials were passed through a Dowex 1 × 2, (chloride form, CH_3OH: H_2O = 1:4), and finally purified by silica gel column chromatography ($CHCl_3$:CH_3OH:H_2O = 10:1:0.1), to give pure *N*-allyl-ACM (71.0 mg, yield 26%) as an orange powder.

HRMS (ESI$^+$ mode): *m/z* 852.38267 (observed), *m/z* 852.38010 (calcd. for $C_{45}H_{58}NO_{15}^+$); ^{1}H-NMR of rhodosamine and D-ring moieties (chemical shift in p.p.m., splitting pattern, *J* in Hz) in $CDCl_3$: H-7 (5.12, d, 5.5), H-8a (2.15, d, 15.0), H-8b (2.58, dd, 5.5 and 15.0), 9-OH (4.76, br s), H-10 (4.06, s), H-13a (1.69, dq, 7.5 and 15.0), H-13b (1.76, dq, 7.5 and 15.0), H-14 (1.15, t, 7.5), -COOMe (3.67, s), H-1′ (5.78, br d, 2.0), H-2′a (overlapping at around 2.1 p.p.m.), H-2′b (overlapping at around 2.3 p.p.m.), H-3′ (5.08-5.14, m), H-4′ (4.44, br s), H-5′ (4.61, q, 7.0), H-6′ (1.36, d, 7.0). *Optical rotation*: $[\alpha]_D^{27}$ −1.7(*c* 0.1, $CHCl_3$) NMR table of *N*-allyl-ACM is presented in Table 1.

In vitro FTase assay

In vitro FTase assay was carried out according to the procedures previously described.[5] In brief, the standard reaction mixture of FTase contained the following components in a final volume of 60 µl:10 µg of partially purified FTase from human esophageal tumor EC17 cells, 10 µg of recombinant GST-H-Ras protein, 0.06 µM of (^{3}H)-farnesyl pyrophosphate (FPP) (596 GBq mmol^{-1}; New England Nuclear, Boston, MA, USA), 50 mM Tris–HCl (pH 7.5, Sigma, St Louis, MO, USA), 50 µM $ZnCl_2$ (Kanto Chemical Co., Tokyo, Japan), 4 mM $MgCl_2$ (Wako Pure Chemical Industries Ltd, Osaka, Japan) and 4 mM DTT (Wako). The reaction was initiated by the addition of enzyme and incubated for 1 h at 37 °C. The reaction was stopped by the addition of 0.5 ml of 1% sodium dodecyl sulfate (SDS, Wako) in MeOH and 0.5 ml of 30% trichloroacetic acid (TCA, Wako). The mixture was then filtered through a Whatman GF/C filter (GE Healthcare, Buckinghamshire, UK), washed with 5 ml of 6% TCA. The dried filter was finally placed in a liquid scintillation counter (Beckman Coulter, Inc., Miami, FL, USA). A blank value was determined in a parallel incubation with boiled enzymes and was subtracted before calculating percent inhibition.

Detection of H-Ras translocation to plasma membrane

Human epidermoid carcinoma A431 cells (1 × 10^6) were seeded in 10 cm dishes and cultured overnight. After the culture supernatant was replaced with DMEM (Nissui Pharmaceutical, Tokyo, Japan) supplemented with 0.2% calf serum, the cells were pretreated with drugs for 15 min and stimulated with 30 ngml^{-1} epidermal growth factor (EGF, Sigma). Following 24 h of incubation, cells were collected and resuspended in buffer A (20 mM Hepes (Sigma), pH 7.5, 10 mM KCl (Kanto Chemical), 1.5 mM $MgCl_2$, 1 mM EDTA (Kanto Chemical), 1 mM EGTA (Wako) and 1 mM DTT containing 250 mM sucrose (Sigma) and 1 mM phenylmethylsulfonyl fluoride (PMSF, Sigma). The cells were homogenized and unbroken cells were removed by centrifuging the homogenates at 1,000 × g for 10 min at 4°C. The supernatant was centrifuged at 100 000 × g for 1 h at 4 °C. The supernatant was removed and the pellets were lysed in radioimmunoprecipitation assay buffer buffer (25 mM Hepes, 1.5% Triton X-100 (Wako), 1% sodium deoxycholate (Wako), 0.1% SDS, 0.5 M NaCl (Wako), 5 mM EDTA, 50 mM NaF (Sigma), 0.1 mM sodium vanadate (Sigma) and 1 mM PMSF, pH 7.8) with sonication. The lysates were centrifuged at 100 000 × *g* for 15 min at 4 °C to give the plasma membrane fraction. The cells were also directly lysed in radioimmunoprecipitation assay buffer buffer with sonication, and the resultant samples were used as the total cell lysate. All samples were subjected to western blotting to detect H-Ras protein.

Transwell migration assay

Cell migration was assayed with a chemotaxis chamber (Becton Dickinson, Franklin Lakes, NJ, USA). A431 cells (7.5 × 10^4) suspended in DMEM supplemented with 0.2% calf serum were incubated in the upper chamber; the lower chamber contained DMEM supplemented with 0.2% calf serum in the presence or the absence of EGF (30 ngml^{-1}). Drugs were added to both chambers. Following 24 h of incubation, the filter was fixed with MeOH and stained with hematoxylin (Sigma). The cells attached to the lower side of the filter were counted.

RESULTS AND DISCUSSION

Screening for inhibitors of FTase

We evaluated the inhibitory activity of compounds against FTase in the project of the SCADS. SCADS is offering several biological activity evaluation of synthesized or isolated compounds for Japanese chemists. For the *in vitro* FTase assay, FTase was partially purified from human esophageal tumor EC17 cells and recombinant GST-H-Ras and (^{3}H)-FPP were used as the substrates. We firstly investigated the effect of compounds on FTase activity at the concentration of 10 µM. As a result, two compounds were found to have inhibitory activity against FTase. As shown in Figure 1, these are novel derivatives of ACM, and were named *N*-benzyl-ACM and *N*-allyl-ACM, respectively. ACM was discovered from a culture of *Streptomyces galilaeus*, and it showed potent antitumor activity.[6,7]

Effect of *N*-benzyl-ACM and *N*-allyl-ACM on FTase activity

In the next step, we examined the inhibitory activities of these ACM derivatives to give IC_{50} values. As shown in Figure 2, *N*-benzyl-ACM and *N*-allyl-ACM inhibit FTase activity in a dose-dependent manner, and the IC_{50} values of *N*-benzyl-ACM and *N*-allyl-ACM were 0.86 and 2.93 µM, respectively (Table 2). On the other hand, ACM did not inhibit FTase activity at a concentration of 10 µM in the process of the screening project of SCADS. Interestingly, neither the C-10 epimer of *N*-benzyl-ACM (10-epi-*N*-benzyl-ACM, see Supplementary Information) nor the C-10 epimer of *N*-allyl-ACM (10-epi-*N*-allyl-ACM, see Supplementary Information) showed an inhibitory effect against FTase activity at a concentration of 10 µM. These results indicated that both modification of the *N*-dimethyl group and the configuration of C-10 are critical for the inhibitory activity of *N*-benzyl-ACM and *N*-allyl-ACM toward FTase. Like FTase, geranylgeranyl transferase (GGTase) catalyzes the geranylgeranylation of proteins terminating with a CAAX motif, where X is restricted to leucine, isoleucine or phenylalanine. FTase and GGTase have been shown to be heterodimers that share a common α subunit with a different β subunit; therefore, we examined the effect of *N*-benzyl-ACM and *N*-allyl-ACM on the inhibitory activity against GGTase and

Table 1 ^{13}C- and ^{3}H-NMR data for N-benzyl-ACM and N-allyl-ACM

Position	δ_H	*mult.*		*J*	*Position*	δ_C
N-benzyl-ACM						
H-1	7.75	1H	dd	1.5Hz, 7.5Hz	C-1	120.1
H-2	7.64	1H	dd	7.5Hz, 8Hz	C-2	137.4
H-3	7.25	1H	dd	1.5Hz, 8Hz	C-3	124.7
					C-4	162.4 or 162.5
					C-4a	115.7
					C-5	192.7
					C-5a	114.4
					C-6	162.4 or 162.5
					C-6a	132.1 or 132.3
H-7	5.18	1H	d	5.5Hz	C-7	69.25 or 69.33
H-8a	2.20	1H	d	15Hz	C-8	36.5
H-8b	2.61	1H	dd	5.5Hz, 15Hz		
					C-9	70.4
H-10	4.12	1H	s		C-10	55.6
					C-10a	143.9
H-11	7.68	1H	s		C-11	121.2
					C-11a	132.1 or 132.3
					C-12	181.2
					C-12a	133.4
H-13a	1.69	1H	dq	7.5Hz, 15Hz	C-13	32.6
H-13b	1.79	1H	dq	7.5Hz, 15Hz		
H-14	1.15	3H	t	7.5Hz	C-14	6.98
H-1′	5.81	1H	brd	~2Hz	C-1′	99.0
H-2′a	2.02–2.17	1H	m		C-2′	26.5
H-2′b	2.35–2.45	1H	m			
H-3′	5.13	1H	brd	~14Hz	C-3′	67.2
H-4′	4.45	1H	brs		C-4′	76.1
H-5′	4.52–4.60	1H	m		C-5′	69.25 or 69.33
H-6′	1.38	3H	d	7Hz	C-6′	18.1
H-1″	5.31	1H	t	4Hz	C-1″	98.3
H-2″a,b	2.02–2.17	2H	m		C-2″	34.8
H-3″	4.05–4.13	1H	m		C-3″	66.0
H-4″	3.80	1H	t	3Hz	C-4″	78.5
H-5″	4.05–4.13	1H	m		C-5″	69.5
H-6″	1.27	3H	d	7Hz	C-6″	16.3
H-1‴	5.09	1H	t	6Hz	C-1‴	98.9
H-2‴a	2.02–2.17	1H	m		C-2‴	27.7
H-2‴b	2.35–2.45	1H	m			
H-3‴	2.44–2.53	2H	m		C-3‴	33.3
					C-4‴	209.6
H-5‴	4.44	1H	q	7Hz	C-5‴	71.7
H-6‴	1.31	3H	d	7Hz	C-6‴	14.8
4-OH	11.98	1H	s			
6-OH	12.78	1H	brs			
9-OH	4.57	1H	brs			
3″-OH	3.45	1H	d	6Hz		
COOMe	3.69	3H	s		COOMe	52.4
					COOMe	171.3
					Bzl-1	127.1
H-Bzl-2	7.41	2H	d	7.8Hz	Bzl-2	133.2
H-Bzl-3	7.19	2H	t	7.8Hz	Bzl-3	129.0
H-Bzl-4	7.32	1H	t	7.8Hz	Bzl-4	130.6
H-BzlCH_2a	4.60	1H	d	12.5Hz	Bzl-CH_2	66.6
H-BzlCH_2b	5.11	1H	d	12.5Hz		
N-Mea	3.08	3H	s		N-Mea	47.2
N-Meb	3.27	3H	s		N-Meb	46.6

Table 1 (Continued)

Position	δ_H	*mult.*		*J*	*Position*	δ_C
N-allyl-ACM						
H-1	7.68	1H	d	8Hz	C-1	120.1
H-2	7.60	1H	t	8Hz	C-2	137.5
H-3	7.20	1H	d	8Hz	C-3	124.8
					C-4	162.4 or 162.5
					C-4a	115.6
					C-5	181.1
					C-5a	114.3
					C-6	162.4 or 162.5
					C-6a	132.1 or 132.3
H-7	5.12	1H	d	5.5Hz	C-7	69.1
H-8a	2.15	1H	d	15Hz	C-8	36.4
H-8b	2.58	1H	dd	5.5Hz, 15Hz		
					C-9	70.3
H-10	4.06	1H	s		C-10	55.7
					C-10a	144.0
H-11	7.50	1H	s		C-11	121.2
					C-11a	132.1 or 132.3
					C-12	192.6
					C-12a	133.2
H-13a	1.69	1H	dq	7.5Hz, 15Hz	C-13	32.7
H-13b	1.76	1H	dq	7.5Hz, 15Hz		
H-14	1.15	3H	t	7.5Hz	C-14	7.1
H-1′	5.78	1H	brd	~2Hz	C-1′	98.9
H-2′a	2.03–2.16	1H	m		C-2′	26.2
H-2′b	2.22–2.36	1H	m			
H-3′	5.08–5.14	1H	m		C-3′	67.8
H-4′	4.44	1H	brs		C-4′	76.2
H-5′	4.61	1H	q	7Hz	C-5′	69.1
H-6′	1.36	3H	d	7Hz	C-6′	18.1
H-1″	5.28	1H	t	3.5Hz	C-1″	98.7
H-2″a,b	2.03–2.16	2H	m		C-2″	34.8
H-3″	4.06–4.13	1H	m		C-3″	66.0
H-4″	3.81	1H	t	2.5Hz	C-4″	78.6
H-5″	3.97–4.06	1H	m		C-5″	69.5
H-6″	1.28	3H	d	7Hz	C-6″	16.5
H-1‴	5.10	1H	t	6Hz	C-1‴	98.9
H-2‴a	2.03–2.16	1H	m		C-2‴	27.8
H-2‴b	2.38–2.54	1H	m			
H-3‴a,b	2.38–2.54	2H	m		C-3‴	33.3
					C-4‴	209.8
H-5‴	4.46	1H	q	7Hz	C-5‴	71.8
H-6‴	1.32	3H	d	7Hz	C-6‴	14.9
4-OH	11.93	1H	s			
6-OH	12.73	1H	brs			
9-OH	4.76	1H	brs			
3″-OH	3.5	1H	brd	6Hz		
COOMe	3.67	3H	s		COOMe	52.4
					COOMe	171.3
Allyl-1a	3.97–4.06	1H	m		C-Allyl-1	64.5
Allyl-1b	4.39	1H	dd	6Hz,13Hz		
Allyl-2	5.88–5.97	1H	m		C-Allyl-2	124.5
Allyl-3a	5.59	1H	d	17Hz	C-Allyl-3	129.8
Allyl-3b	5.62	1H	d	10Hz		
N-Mea	3.15	3H	s		NMea	47.6
N-Meb	3.24	3H	s		NMeb	47.4

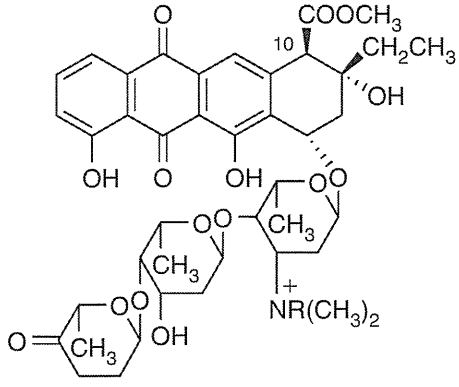

Aclacinomycin A (ACM); R=H
N-benzyl-ACM; R=$CH_2C_6H_5$
N-allyl-ACM; R=$CH_2CH{=}CH_2$

Figure 1 Structures of ACM derivatives.

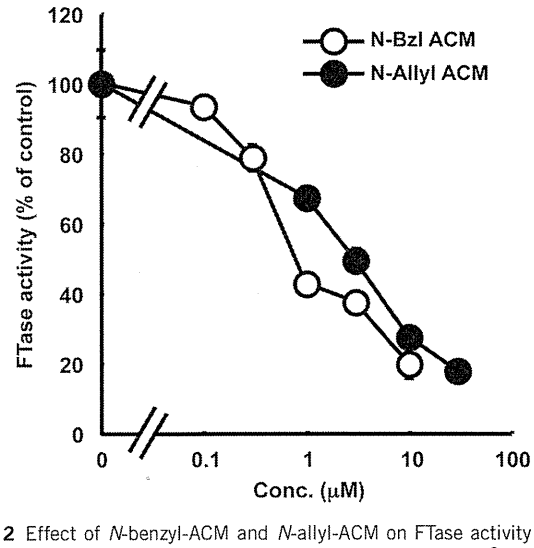

Figure 2 Effect of *N*-benzyl-ACM and *N*-allyl-ACM on FTase activity *in vitro*. Partially purified FTase from EC17 cells was incubated with (^{3}H)-FPP plus recombinant GST-H-Ras in the presence or absence of *N*-benzyl-ACM (*N*-Bzl-ACM) or *N*-allyl-ACM (*N*-Allyl-ACM). The reaction was terminated by the addition of TCA. The radioactivity of the TCA-insoluble fraction was measured. The results are the mean ± s.d. of two independent experiments.

Table 2 Effect of *N*-benzyl-ACM and *N*-allyl-ACM on FTase, GGTase and GGPP synthase activities *in vitro*, as well as cell migration and cell viability in A431 cells

	IC_{50} (μM)	
	N-benzyl-ACM	*N-allyl-ACM*
FTase	0.86	2.93
GGTase	100	>100
GGPP synthase	>100	>100
Cell migration	0.65	1.55
Cell viability (-EGF)	>10	>30
Cell viability (+EGF)[a]	9.09	22.0

[a]The concentration of EGF was 30 ng ml^{-1}.

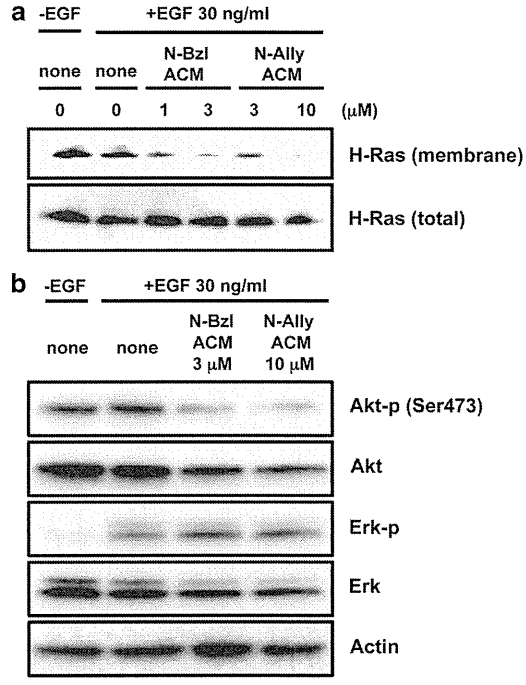

Figure 3 Effect of *N*-benzyl-ACM and *N*-allyl-ACM on H-Ras translocation, phosphorylation of Akt and Erk in A431 cells. (**a**, **b**) A431 cells were pretreated with drugs for 15 min and stimulated with EGF. Following 24 h of incubation, cells were collected and the membrane fraction was extracted (**a**) All samples were subjected to immunoblotting.

found that they failed to inhibit GGTase up to 100 μM. Geranylgeranyl pyrophosphate (GGPP) synthase is an enzyme that catalyzed the synthesis of GGPP from isopentenyl pyrophosphate and FPP; thus, because both FTase and GGPP synthase use FPP as a substrate, the effect of *N*-benzyl-ACM and *N*-allyl-ACM on GGPP synthase activity was examined. However, neither FTase inhibitor could inhibit GGPP synthase up to 100 μM (Table 2). So far, although several anthraquinones have been reported as FTase inhibitors,[8,9] none of the anthracycline family has been identified as an FTase inhibitor; thus, *N*-benzyl-ACM and *N*-allyl-ACM are the first examples in a series of the anthracycline family, demonstrating that the compounds inhibit FTase.

Effect of *N*-benzyl-ACM and *N*-allyl-ACM on localization of H-Ras

Because *N*-benzyl-ACM and *N*-allyl-ACM selectively inhibited FTase *in vitro*, next we examined whether these compounds could inhibit FTase in a cultured cell system. A431 cells were well-known EGF receptor-overexpressing cells that displayed a sufficient level of H-Ras protein[10] As shown in Figure 3a, the amount of H-Ras in the membrane fraction was not changed in the presence or absence of EGF; however, treatment of cells with *N*-benzyl-ACM and *N*-allyl-ACM reduced the amount of H-Ras in the membrane fraction. On the other hand, *N*-benzyl-ACM and *N*-allyl-ACM did not affect the geranylgeranylation of Rap1A in the same condition (data not shown). These results suggested that *N*-benzyl-ACM and *N*-allyl-ACM inhibited the membrane localization of H-Ras protein through the inhibition of FTase in A431 cells.

Effect of *N*-benzyl-ACM and *N*-allyl-ACM on PI3K signaling

The activation of H-Ras was reported to further activate the PI3K pathway.[11,12] Indeed, we previously reported that other FTase

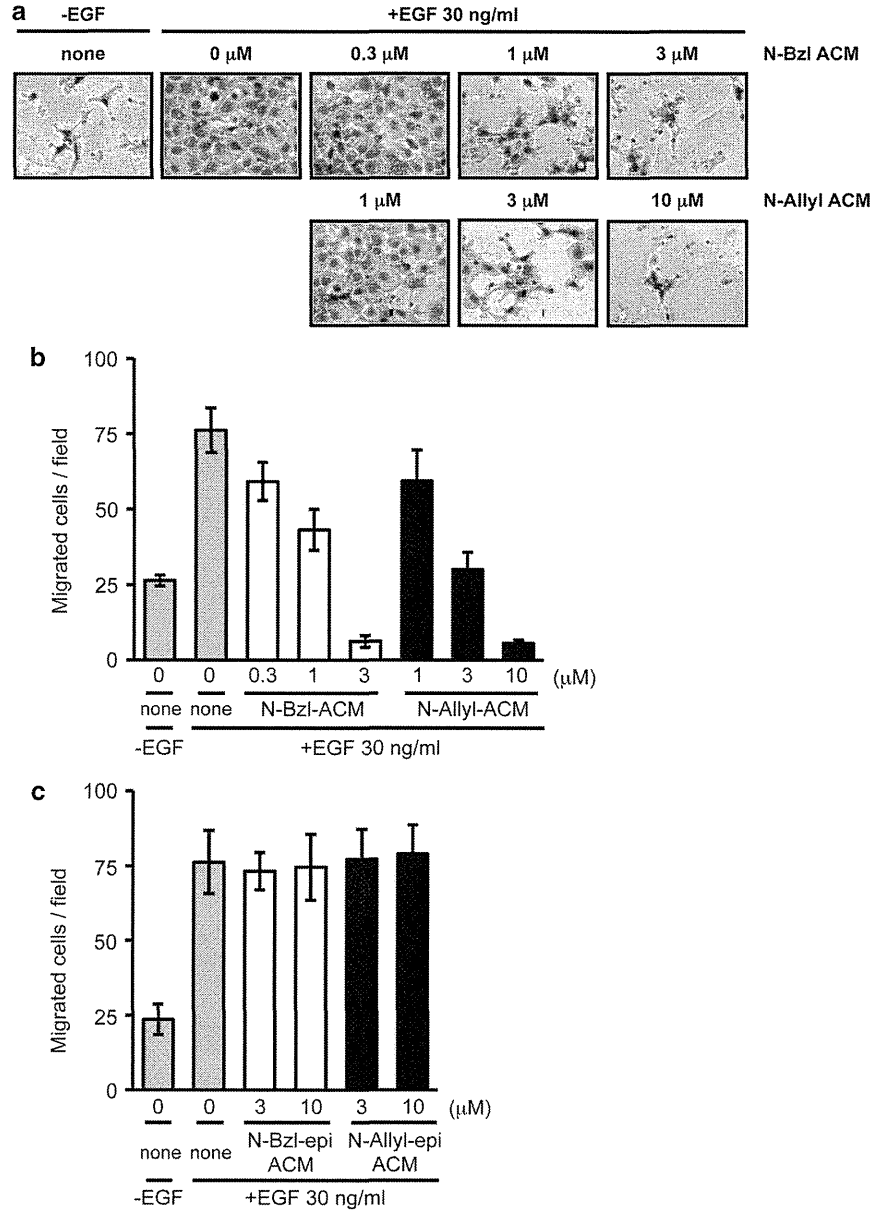

Figure 4 Effect of *N*-benzyl-ACM and *N*-allyl-ACM on EGF-induced cell migration in A431 cells. A431 cells suspended in DMEM supplemented with 0.2% calf serum were incubated in the upper chamber; the lower chamber contained DMEM supplemented with 0.2% calf serum in the presence or absence of EGF (30 ng ml^{-1}). Drugs were added to both chambers. After 24 h, the cells that migrated through the filter to the lower surface were photographed (**a**), and the number of migrated cells was counted (**b**, **c**). The results are the mean ± s.d. of five different fields.

inhibitors, moverastin A and B, inhibited the PI3K/Akt pathway but not the Raf/MEK/Erk pathway.[5] To confirm whether *N*-benzyl-ACM or *N*-allyl-ACM also could inhibit the PI3K pathway selectively, we examined the effect of these compounds on the phosphorylation of Akt or Erk in A431 cells. As shown in Figure 3b, the phosphorylation of Akt (Ser473) was significantly decreased in the presence of either *N*-benzyl-ACM or *N*-allyl-ACM, whereas these compounds did not affect the phosphorylation level of Erk. These results suggested that *N*-benzyl-ACM and *N*-allyl-ACM inhibited PI3K activation through the suppression of H-Ras farnesylation.

Effect of *N*-benzyl-ACM and *N*-allyl-ACM on cell migration

Since the activation of H-Ras through the farnesylation by FTase was involved in cell migration,[5] we examined the effect of N-benzyl-ACM or *N*-allyl-ACM on EGF-induced cell migration in A431 cells. As a result, *N*-benzyl-ACM or *N*-allyl-ACM inhibited EGF-induced cell migration in a dose-dependent manner (Figures 4a, b). These inhibitory effects were not due to the toxic effect of the drugs because their IC_{50} values for A431 cell viability were at least seven times higher than those for cell migration (Table 2). Importantly, the dose of *N*-benzyl-ACM or *N*-allyl-ACM required to inhibit cell migration was consistent with that for inhibition of the membrane localization of H-Ras. Moreover, according to the inhibitory activity against FTase, the IC_{50} value for the cell migration of *N*-benzyl-ACM was lower than that of *N*-allyl-ACM (Table 2). Neither 10-epi-*N*-benzyl-ACM nor 10-epi-*N*-allyl-ACM, which failed to inhibit FTase, suppressed EGF-induced migration of A431 cells (Figure 4c). Taken together, these findings suggest that *N*-benzyl-ACM and *N*-allyl-ACM inhibited

the EGF-induced migration of A431 cells by inhibiting H-Ras farnesylation.

CONFLICT OF INTEREST

The authors declare no conflict of interest.

ACKNOWLEDGEMENTS

We would like to thank MicroBiopharm Japan Co., Ltd. (formerly Mercian Corp.) for kind gift of ACM. This study was supported by KAKENHI (60200854), and the SCADS was supported by a Grant-in-Aid for Scientific Research on Priority Area 'Cancer' from The Ministry of Education, Culture, Sports, Science and Technology, Japan.

1 Gupta, G. P. & Massagué, J. Cancer metastasis: building a framework. *Cell* **127,** 679–695 (2006).
2 Fox, P. L., Sa, G., Dobrowolski, S. F. & Stacey, D. W. The regulation of endothelial cell motility by p21 ras. *Oncogene* **9,** 3519–3526 (1994).
3 Ridley, A. J., Comoglio, P. M. & Hall, A. Regulation of scatter factor/hepatocyte growth factor responses by Ras, Rac and Rho in MDCK cells. *Mol. Cell Biol.* **15,** 1110–1122 (1995).
4 Rowinsky, E. K., Windle, J. J. & Hoff Von, D. D. Ras protein farnesyltransferase: a strategic target for anticancer therapeutic development. *J. Clin. Oncol.* **17,** 3631–3652 (1999).
5 Takemoto, Y. *et al.* Chemistry and biology of moverastins, inhibitors of cancer cell migration, produced by *Aspergillus. Chem. Biol.* **12,** 1337–1347 (2005).
6 Oki, T., Matsuzawa, Y., Yoshimoto, A., Numata, K. & Kitamura, I. New antitumor antibiotics aclacinomycins A and B. *J. Antibiot.* **28,** 830–834 (1975).
7 Hori, S. *et al.* Antitumor activity of new anthracycline antibiotics, aclacinomycin-A and its analogs, and their toxicity. *Jpn. J. Cancer Res.* **68,** 685–690 (1977).
8 Sekizawa, R. *et al.* Isolation of novel saquayamycins as inhibitors of farnesyl-protein transferase. *J. Antibiot.* **49,** 487–490 (1996).
9 Kwon, B.-M. *et al.* Farnesyl protein transferase inhibitory components of polygonum multiflorum. *Arch. Pharm. Res.* **32,** 495–499 (2009).
10 Sawada, M. *et al.* Synthesis and anti-migrative evaluation of moverastin derivatives. *Bioorg. Med. Chem. Lett.* **21,** 1385–1389 (2011).
11 Engelman, J. A. Targeting PI3K signalling in cancer: opportunities, challenges and limitations. *Nat. Rev. Cancer* **9,** 550–562 (2009).
12 Rodriguez-Viciana, P., Warne, P. H., Vanhaesebroeck, B., Waterfield, M. D. & Downward, J. Activation of phosphoinositide 3-kinase by interaction with Ras and by point mutation. *EMBO J.* **15,** 2442–2451 (1996).

Supplementary Information accompanies the paper on The Journal of Antibiotics website (http://www.nature.com/ja)

SCIENTIFIC REPORTS

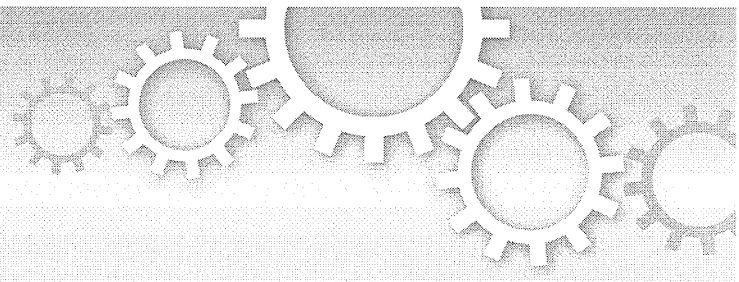

OPEN

SUBJECT AREAS:
CHEMICAL BIOLOGY
CANCER
COLLECTIVE CELL MIGRATION
MESENCHYMAL MIGRATION

Received
22 August 2012

Accepted
17 October 2012

Published
8 November 2012

Correspondence and requests for materials should be addressed to M.I. (imoto@bio.keio.ac.jp)

A chemical genomic study identifying diversity in cell migration signaling in cancer cells

Shigeyuki Magi, Etsu Tashiro & Masaya Imoto

Department of Biosciences and Informatics, Faculty of Science and Technology, Keio University, 3-14-1 Hiyoshi, Kohoku-ku, Yokohama 223-8522, Japan.

The aim of this study was to analyze the diversity and consistency of regulatory signaling in cancer cell migration, using a chemical genomic approach. The effects of 34 small molecular compounds were assessed quantitatively by wound healing assay in ten types of migrating cells. Hierarchical clustering was performed on the subsequent migration inhibition profile of the compounds and cancer cell types. The result was that hierarchical clustering accurately classified the compounds according to their targets. Furthermore, the cancer cells tested in this study were classified into three clusters, and the compounds were grouped into four clusters. An inhibitor of JNK suppressed all types of cell migration; however, inhibitors of ROCK, GSK-3 and p38MAPK only inhibited the migration of a subset of cell lines. Thus, our analytical system could easily distinguish between the common and cell type-specific signals responsible for cell migration.

Cell migration is central to many physiological processes, including development, tissue remodeling, and immune responses, and is also a required step in cancer metastasis. When a cell moves, multiple intracellular signaling networks control cell morphology. Signaling can be initiated through receptor tyrosine kinases, G protein-coupled receptors (GPCRs), integrin, and other receptors. These receptors are upregulated by extracellular stimuli that induce the activation of one or more intermediate signaling network branches. Finally, this signaling reaches the Rho family of small GTPase proteins. Many molecules and pathways have been implicated in intermediate signaling. For example, the Ras/Raf/MEK/ERK pathway has been reported to enhance cell motility[1–4]. In addition to the Ras/Raf/MEK/ERK pathway, a phosphoinositide 3-OH kinase (PI3K)/Akt pathway is widely known to regulate cell migration. This pathway is considered to be necessary for both Cdc42- and Rac1-induced cell motility and invasiveness[5], and it regulates the expression of Snail, which can increase cell motility[6]. Jun NH2-terminal kinase (JNK) and p38 mitogen-activated protein kinase (p38MAPK) have also been reported to play important roles in the signaling mechanisms involved in migration[7,8]. The role of Rho family small GTPase proteins, which is considered to constitute the final stage of the migration-signaling network, is known to regulate actin nucleation and polymerization. In particular, RhoA, Rac1, and Cdc42 are the major regulators of cytoskeletal remodeling. Activation of RhoA increases cell contractility and leads to the formation of focal adhesions and stress fibers[9]. Rac1 and Cdc42 activation induce the lamellipodia and filopodia, respectively[10,11]. Thus, the core elements of the intracellular migration-signaling network have been demonstrated.

However, it is likely that signaling molecules regulating cell migration in one cancer cell may not regulate cell migration in other genetically distinct cancer cells. Indeed, the PI3K/Akt pathway, but not the MEK/ERK pathway, has been shown to be critical for prostate cancer cell migration[6]. Other studies have reported that the constitutive activation of the MEK/ERK pathway by oncogenic mutations of $BRaf^{V600E}$ significantly induced cell migration through activation of RhoA GTPase[12]. In addition, the role of the Rho family of proteins in cell migration depends on specific cellular circumstances. The migration of several types of cancer cell is based on reorganization of the actin cytoskeleton, but their requirements for Rho and Rac signaling differ. With respect to a particular subset of cancer cells, cells migrated in a Rac-dependent manner, but Rho signaling was not essential. With respect to another subset of cancer cells, the inhibition of Rho/Rock signaling inhibited cell migration. Thus, although the same basic process of cell migration is induced, each type of cancer cell brings about migration in different contexts using distinct molecular repertoires. Therefore, understanding the diversity and commonality of signaling pathways that regulate cell migration in various cell types is important not only for basic research into cell migration, but also for the development of anti-metastatic anti-tumor drugs.

Table 1 | The experimental conditions of the wound healing assays for each cell line

Cell line	Origin	Cell number (cells/well)	Migration factor
A431	Human epithelial carcinoma	7.5×10^4	EGF 3 ng/ml or EC17-CM
EC17	Human esophageal carcinoma	7.5×10^4	None
EC109	Human esophageal carcinoma	7.5×10^4	EGF 3 ng/ml or EC17-CM
HT1080	Human fibrosarcoma	7.5×10^4	FBS (2%)
TE8	Human esophageal carcinoma	7.5×10^4	EGF 3 ng/ml
TT	Human medullary thyroid carcinoma	7.5×10^4	EGF 3 ng/ml
3Y1	Rat fibroblast	7.5×10^4	FBS (5%)
B16	Mouse melanoma	2.2×10^5	EC17-CM

To address this issue, we utilized the chemical genomic approach in which chemical inhibitors were used as probes to mimic loss-of-function phenotypes by inhibiting target protein activity; that is, if a chemical inhibitor suppresses the cell migration of one type of cancer cell, the target protein of the inhibitor can be considered as being involved in the mechanism of cell migration of that type of cell. This chemical genetic approach is easily applicable to different cell models; therefore, it can determine which signaling molecule is universally involved in the migration mechanism in several types of cancer cells, and which one is specifically involved in each type of cell. In the present study, we first examined the effects of various chemical inhibitors on cell migration in several cancer cell models, and subsequently obtained chemosensitive migratory profiles and undertook cluster analysis to classify the signaling molecules and their inhibitors as being either common to all cancer cells or specific to certain cell types.

Results

Determination of appropriate experimental conditions for the wound healing assay. To select the cell models used in this study, sixteen cell lines, including colon carcinoma, esophageal carcinoma and lung cancer, were assessed with regard to their migration ability in response to migration factors using a wound healing assay[13]. The assay conditions of each cell line were optimized by examining migration factors such as growth factors, cell number required to maintain a confluent cell monolayer, and an assay duration that clearly revealed the extent of motility. We found out that the eight cell lines were suitable for use in a migration assay under the conditions indicated in **Table 1** (see also the Methods section). We also confirmed that both number of alive and dead cells in each condition were not clearly increased in optimized assay condition. The other cell lines tested were not affected by migratory stimuli or could not be scratched. Among the eight cell lines selected, EC17 cells migrated without extracellular stimulation, indicating that EC17 cells secrete chemoattractants into the media, and acquire motility by autocrine signaling. Conversely, others required the addition of migration factors, such as epidermal growth factor (EGF), conditioned medium from EC17 cells (EC17-CM), or serum (**Figure 1a**). A431 cells and EC109 cells migrated in response to both EGF and EC17-CM. **Figure 1b** shows the morphology of migration in these cell lines. A431 cells and EC109 cells moved together in sheet-like structures (collective migration), whereas the other cell lines showed a fibroblast-like spindle-shaped morphology and migrated individually like mesenchymal cells (mesenchymal migration).

Signaling pathway regulating for cell migration differs among three cancer cell lines. Next, to examine whether our analytical system could distinguish between common signals responsible for cell migration in the cancer cells tested and cell type-specific signals, using signal transduction inhibitors, a test was done using A431 cells, EC109 cells or TT cells that were randomly selected to analyze their migration ability. This was conducted following treatment with three

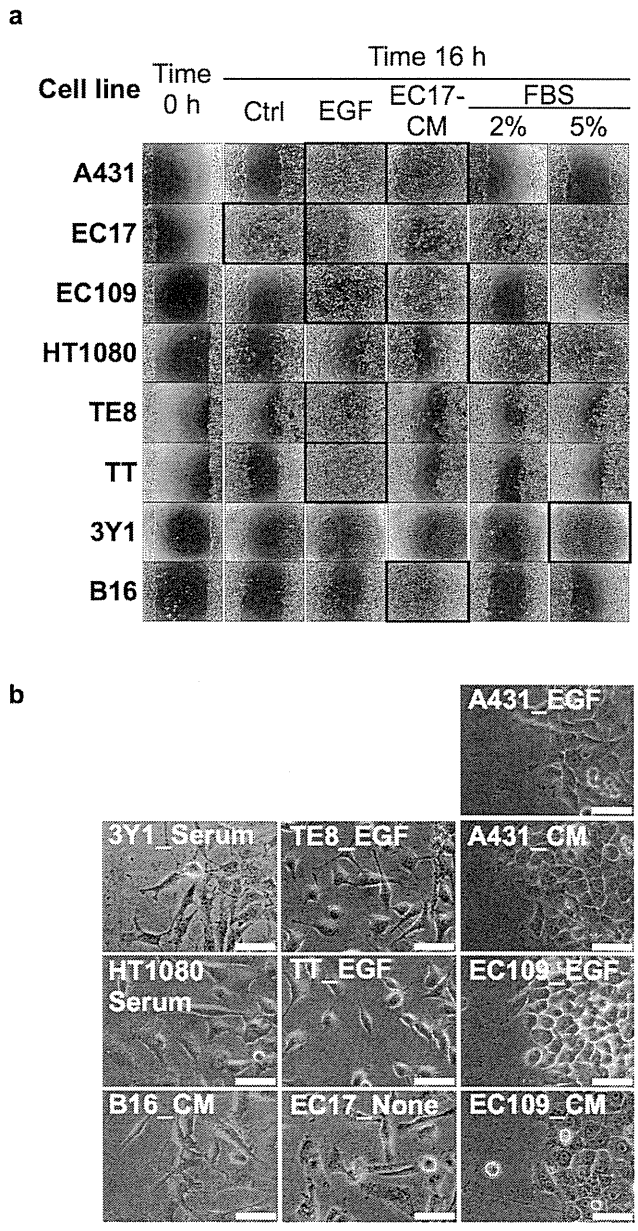

Figure 1 | The effect of migratory stimuli on cell migration in various cell lines. (a) Cells were scratched and then stimulated by EGF (3 ng/mL), serum, or conditioned medium from EC17 cells. After 16 h, wound areas were observed and photographed under microscopy. (b) Images of cell lines treated with migratory stimuli. Cells were photographed 10 h after stimulation. The scale bar represents 50 μm.

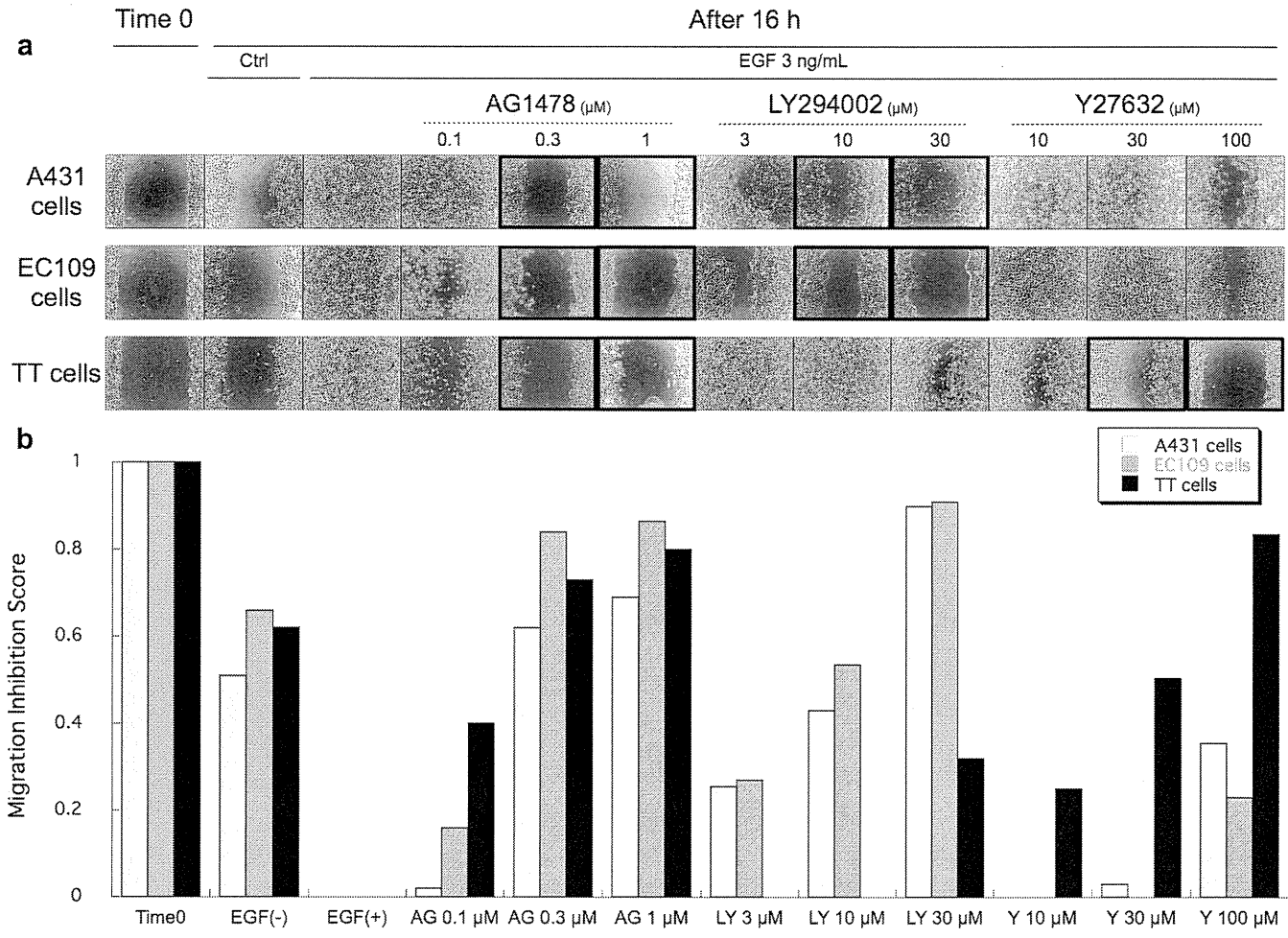

Figure 2 | The inhibitory pattern of cell migration was dependent on the types of cancer cell line. A confluent monolayer of A431 cells, EC109 cells, and TT cells were scratched, treated with AG1478, LY294002, or Y27632, and stimulated with EGF as described in the Methods section. (a) Wound areas were photographed just after scratching (time zero). After 16 h, wound areas were photographed again (others). Black boxes indicate the inhibitory effects of chemicals on cell migration. The data were representative of two independent studies. (b) Migration inhibition score (MIS) of each experimental condition. MIS was quantified by measurement of the cell-free area in the picture. The quantified value was normalized against the value at time zero. The data were the average of two independent studies.

kinase inhibitors; PI3K inhibitor, Rho-associated kinase (ROCK) inhibitor and EGF receptor kinase inhibitor. The reason why we focused on the inhibitors of PI3K and ROCK for this test was that PI3K and ROCK were expected to reveal cell type-specific effects on migration. This is because they have been reported to be involved in regulation mechanisms of cell migration that are initiated downstream to growth factor signaling in a subset of cancer cells[5,14], although they were also reported to be dispensable for migration or membrane ruffling in certain conditions[15,16]. **Figure 2a** presents the effect of these three inhibitors on the EGF-induced motility of A431 cells, EC109 cells, and TT cells. The extent of the cell motility was quantified by the measurement of the cell-free area in a photograph. The quantified value was calculated over a fixed period of time, and was termed the 'migration inhibition score (MIS)' (**Figure 2b**). These results indicated that the EGF receptor kinase inhibitor, AG1478, inhibited the EGF-induced migration of all three cell lines, as expected. The PI3K inhibitor and LY294002 suppressed the EGF-induced migration of A431 cells and EC109 cells, but not of TT cells, indicating that PI3K plays a critical role in EGF-induced cell migration in A431 cells and EC109 cells. In contrast, the ROCK inhibitor, Y27632, suppressed migration only in A431 cells and TT cells, indicating that ROCK is indispensable for EGF-induced cell migration in A431 cells and TT cells but not in EC109 cells. Thus, our analytical system using chemical inhibitors of signal transduction easily distinguished between common and cell type-specific signals responsible for cell migration.

Two-way cluster analysis of migration inhibition score. To reveal the diversity and generality of regulatory signaling in cancer cell migration, we tested the effect of 34 different signal transduction inhibitors on the migration of ten types of cells, as shown in Table 1. Table 2 lists the names of the chemical inhibitors of signal transduction used in this study, the experimental concentrations of each inhibitor, and their modes of action. Each inhibitor was used at three concentrations, the highest one being a concentration just below the level that would affect cell viability. Using these chemical inhibitors under the stated concentrations, we carried out two highly reproducible, independent experiments on each cell line ($r = 0.94$, p-value $< 2.2 \times 10^{-16}$, **Figure 3**), and provided a final dataset by averaging the data points from the two experiments. The MIS dataset is shown in Supplementary Table 1. Then a hierarchical cluster analysis was performed. The results are displayed in the form of a heat map and a tree diagram (**Figure 4**). The heat map employs a gradient color scale from green, indicating MIS = 0, to magenta, indicating MIS = 1.0, interpolated over black indicating MIS = 0.5.

As a result of these experiments, the characteristic features of cell migration affected by chemical inhibitors in cancer cells were

Table 2 | Compound concentrations and targets of inhibition used in this study

Compound name	Concentration	Target / Mode of action	References
A23187	30, 100, 300 nM	Ca^{2+} Ionophore	33
AA861	3, 10, 30 μM	5-Lipoxygenase	34
AG1478	0.1, 0.3, 1 μM	EGFR	35
Alendronate	10, 30, 100 μM	FPP synthase	36
ALLN	1, 3, 10 μM	Calpain	37
Bafilomycin A	0.3, 1, 3 nM	V-ATPase	38
Cytochalasin D	0.1, 0.3, 1 μM	Actin polymarization	39
Herbimycin A	1, 3, 10 μg/mL	Hsp90	40
Leptomycin B	0.1, 0.3, 1 ng/mL	CRM1	41
LY294002	3, 10, 30 μM	PI3K	42
Mevastatin	3, 10, 30 μM	HMG-CoA reductase	43
Moverastin	3, 10, 30 μM	Farnesyl transferase	20
MG132	10, 30, 100 nM	Proteasome	44
MK571	3, 10, 30 μM	CysLT1	45
MK886	1, 3, 10 μM	FLAP	46
Okadaic acid	3, 10, 30 nM	PP2A	47
Paclitaxel	30, 100, 300 ng/mL	Tubulin depolymerization	48
PD169316	1, 3, 10 μM	p38MAPK	49
Radicicol	1, 3, 10 μg/mL	Hsp90	50
Rapamycin	1, 3, 10 μg/mL	mTOR	51
Risedronate	30, 100, 300 μM	FPP synthase	36
SB203580	3, 10, 30 μM	p38MAPK	52
SB218078	30, 100, 300 nM	Chk1	53
SB415286	3, 10, 30 μM	GSK-3	54
SP600125	1, 3, 10 μM	JNK	55
Thapsigargin	3, 10, 30 nM	Ca^{2+}-ATPase	56
Trichostatin A	30, 100, 300 ng/mL	Histone deacetylase	57
Tunicamycin	30, 100, 300 ng/mL	Glycosylation	58
U0126	3, 10, 30 μM	MEK	59
UTKO1	1, 3, 10 μM	14-3-3	22
Vinblastine	3, 10, 30 ng/mL	Tubulin polymerization	60
Wortmannin	0.3, 1, 3 μM	PI3K	61
Xanthohumol	0.3, 1, 3 μg/mL	Valosin-containing protein	23
Y27632	10, 30, 100 μM	ROCK	62

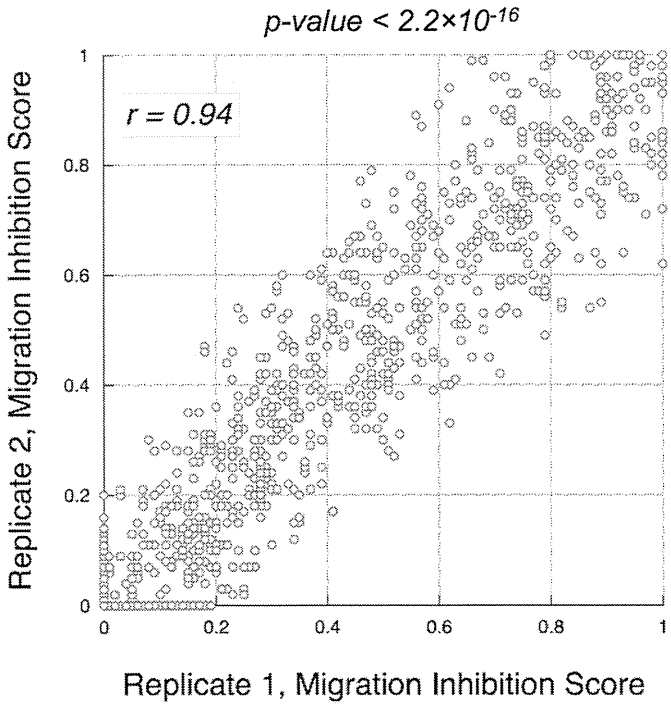

Figure 3 | Reproducibility of the migration inhibition score. Before averaging, two independent data sets were checked for high correlation ($r = 0.94$, p-value $< 2.2 \times 10^{-16}$).

classified into three general clusters (**Figure 4a**). Cluster A consisted of three types of cells and cell migration properties: B16 cells, HT1080 cells, and 3Y1 cells; their cell migration displayed lower sensitivities to the inhibitors tested in this study than the others (**Figure 4b**). Cluster B consisted of cell migration of A431 cells and EC109 cells stimulated with either EGF or EC17-CM. The EGF-induced chemosensitive migratory profile of these cells was similar to that induced by EC17-CM. Cluster C consisted of three types of cells: EC17 cells, TE8 cells and TT cells.

It was expected that the chemical inhibitors that targeted the same molecule would be clustered into the same tree. Indeed, PD169316 and SB203580 as p38MAPK inhibitors, herbimycin A and radicicol (Hsp90 inhibitors), LY294002 and wortmannin (PI3K inhibitors), paclitaxel and vinblastine (tubulin binders), and alendronate and risedronate (farnesyl diphosphate (FPP) synthase inhibitors), were all clustered into the same position (indicated by gray boxes). These results indicate that our chemical genomic approach was able to classify the chemical inhibitors based on their respective modes of action, similar to previous studies on the chemosensitivities of cancer cells[17–19].

Furthermore, the chemical inhibitors used in this study were classified into four general clusters (**Figure 4b**), and each inhibitor in **Figure 4b** can be linked to its target molecule. We also displayed the relationships of the targets of the inhibitors as a non-root phylogenetic tree (**Figure 4c**). The inhibitors grouped into cluster 1 contained the 5-lipoxygenase-activating protein (FLAP) inhibitor, MK886, the vacuolar-type proton-ATPase (V-ATPase) inhibitor, bafilomycin A, and the FPP synthase inhibitors, the bisphosphonates. These inhibitors showed little inhibitory effect on cell migration in almost all cell types, thus the target molecules of these compounds had little bearing

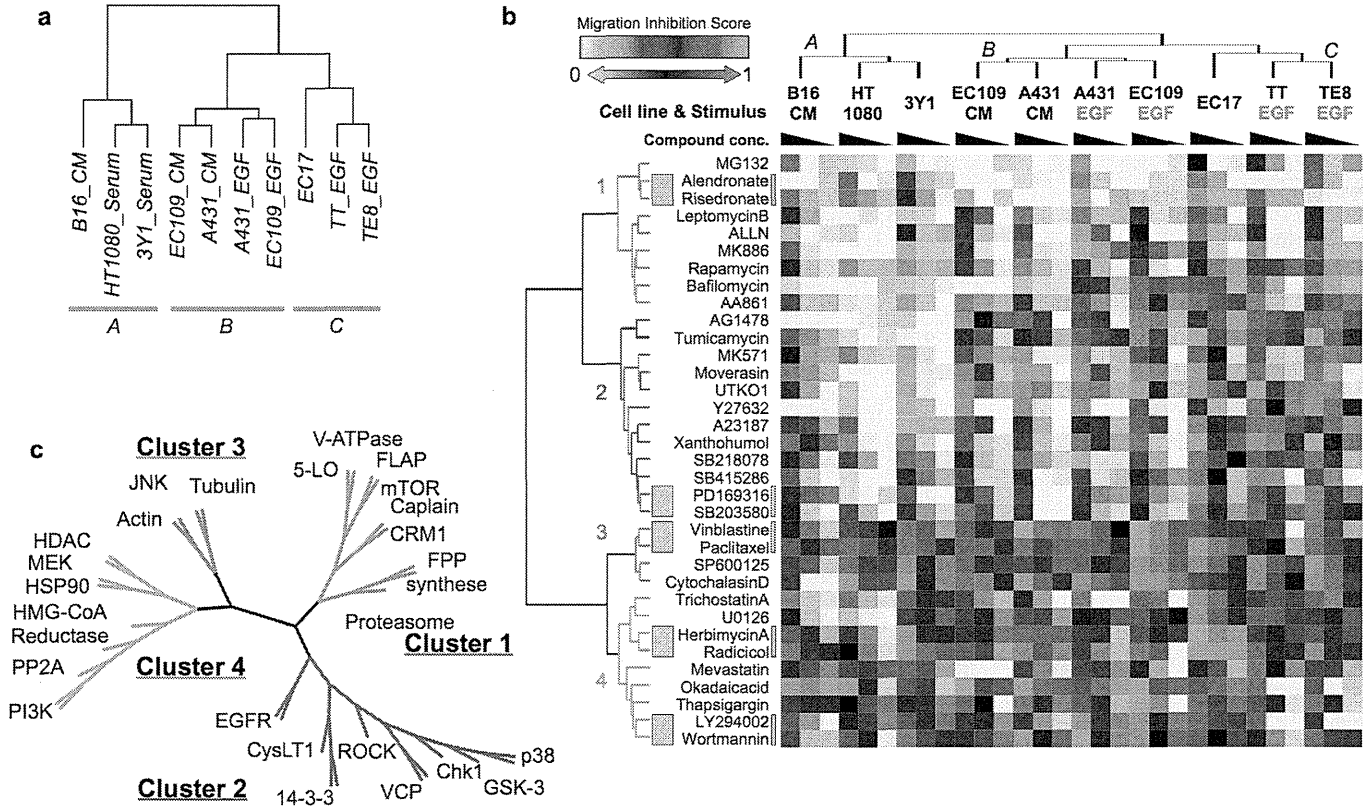

Figure 4 | Cluster analysis of the chemosensitivity profile of migration inhibition. Cluster analysis was performed using Euclidean distance and Ward's method. (a) The MIS dataset was clustered into ten types of cell migration. Cell migration types were classified into three general clusters; clusters A, B, and C. (b) The MIS dataset was hierarchically clustered using data from 34 compounds. Rows indicate 34 different small molecular compounds. Columns indicate the ten migration types, including the three different compound concentrations. The heat map shows a gradient color scale from green, indicating MIS = 0, to magenta, indicating MIS = 1, interpolated over black for MIS = 0.5. Gray boxes beside the heat map indicate that two labeled compounds have almost the same molecular target. The 34 compounds were clustered into four general groups. (c) The non-rooted phylogenetic tree classifies the target molecules of the small molecular compounds tested in this study. Each small compound inhibitor used in this study can be replaced with its target molecule because most targets have already been identified. This phylogenetic tree presents the distances between molecules on the signaling network contributing to cell migration.

on the regulating mechanisms of cell migration tested in this study. Cluster 2 contained Y27632, AG1478, the p38MAPK inhibitors, the chk1 inhibitor, SB218078 and so on. Most of these compounds showed a stronger inhibitory effect on cell migration, classified into migration type clusters B and C, in contrast to cluster A. Therefore, the target molecules of these compounds were not involved in the migration of HT1080 cells and 3Y1 cells but they did regulate cell migration in the subset of cell lines grouped into clusters B and C. Cluster 3 contained SP600125 and the cytoskeleton-affecting compounds. This group of inhibitors affected all types of cell migration, indicating that not only cytoskeletal molecules, but also JNK, are common regulators of cell migration, irrespective of cell type. Cluster 4 contains the Hsp90 inhibitors, the MEK inhibitor, U0126, and the PI3K inhibitors. These inhibitors also suppressed migration in all types of cell with different potencies depending on cell type. Thus the target molecules of these inhibitors also played a common role in all types of cell migration.

Discussion

In the present study, we investigated some general and specific regulatory mechanisms of cell migration. To accomplish our objective, we assessed the effects of 34 different kinds of chemical inhibitors on the migration of ten types of cells using a wound healing assay, and subsequently performed a cluster analysis on the dataset. One significant aspect of this work is that each compound showed a characteristic cell type-specific inhibitory pattern on migration, and hierarchical clustering precisely classified the compounds according to their respective targets, such as p38, Hsp90, PI3K, tubulin and FPP synthase (**Figure 4b, c**). Therefore, our research could be applied to predict the mode of action of each compound. For example, moverastin and its derivative UTKO1 were classified into same cluster, in spite of the different functions of these two compounds, which have similar structures. We previously reported that moverastin was an inhibitor of farnesyltransferase[20], and it inhibited cell migration by inhibiting farnesylation in H-Ras. On the other hand, UTKO1 was reported not to inhibit farnesyltransferase[21], but it directly bound to 14-3-3ζ, and inhibited the interaction between the 14-3-3 proteins and Tiam1, a protein that has been reported to be a Rac-specific GEF. This resulted in the inhibition of Rac1[22]. Therefore, it has been demonstrated that the migration of epithelial cells requires Taim1-mediated Rac1 activation. However, because our profiling data demonstrated that moverastin and UTKO1 were classified in the same cluster, we examined the possibility that moverastin could bind to 14-3-3ζ, and obtained similar results (data not shown). Therefore it is likely that moverastin might inhibit cell migration not only by inhibiting protein farnesylation, but also by inhibiting Tiam1-mediated Rac1 activation. In addition, because the CysLT1 antagonist MK571 was classified into the same cluster as moverastin and UTKO1, this raised the possibility that CysLT1 signaling might be closely related to Taim1-mediated Rac1 activation. We therefore examined this potential mode of action, and found that EGF-induced Rac1 activation was regulated by CysLT1 signaling (unpublished

data). Thus, our profiling data appeared to be helpful in the mechanistic study of cell migration. At the same time, our clustering data indicated that xanthohumol was grouped in the same category as the Ca^{2+} ionophore, A23187. Recently, xanthohumol was reported to bind to and inhibit valosin-containing protein (VCP)[23], resulting in the induction of ER stress. Although A23187 is also a well-known inducer of ER stress[24,25], other ER stress-inducing compounds such as tunicamycin and thapsigargin were classified into different clusters from xanthohumol and A23817. Therefore, an interpretation of the clustering data must be made with great caution.

The characteristics of cell migration based on chemical inhibitor-sensitivity profiles were grouped into three clusters (clusters A, B and C), and chemical inhibitors were classified into four general groups (clusters 1 to 4, **Figure 4**). Although the motilities of several cell lines we tested are upregulated by extracellular stimuli such as EGF, they migrated a little without stimulation (**Figure 1a**). Additionally, EC17 cells did not require extracellular stimulation to migrate. Thus we just have to evaluate and discuss chemical inhibitor-sensitivity profiles as total effects on "basal" and "stimulated" motility. JNK inhibitor, tubulin and actin polymerization inhibitors in cluster 3 showed a potent inhibitory effect on migration of all cell types, indicating that JNK is a common and crucial signaling molecule regulating cell migration. Indeed, JNK was reported to modulate migration in a broad range of cell types[26], such as keratinocytes[7], neuronal cells[27], and many cancer cell lines[28,29]. Because dynamic reorganization of the actin cytoskeleton is considered to be key to the cell's capacity to migrate[30], JNK may be indispensable for the phosphorylation of paxillin and F-actin polymerization[7,8].

In contrast, some of the chemical inhibitors classified into cluster 2 (AG1478, tunicamycin, the CysLT1 antagonist MK571, Moverastin and UTKO1) affected the migration of cell lines of epithelial origin (EC109 cells, A431 cells, EC17 cells, TT cells, TE8 cells) in clusters B and C, but did not affect the migration of cell lines of mesenchymal origin (HT1080 cells and 3Y1 cells) placed in cluster A. This suggests that there is an essentially different regulatory mechanism of cell migration between cells of these two origins. The regulatory mechanism of cell migration of B16 cells appeared somewhat similar to that of cell lines of mesenchymal origin when compared to those with an epithelial origin.

Moreover, although EGF did induce migration of cells of epithelial origin (TT cells, TE8 cells, A431 and EC109 cells), differential sensitivities to several inhibitors was observed in A431 and EC109 cells in cluster B and TT cells and TE8 cells in cluster C. These results suggest that the EGF signaling pathway leading to migration of A431 and EC109 cells in cluster B was not identical to that of TT cells and TE8 cells in cluster C. Furthermore, EC17-CM also induced migration of A431 and EC109 cells with a similar chemosensitive profile to that seen in EGF-induced migration, indicating that EC17-CM might activate almost the same signaling pathway as the EGF-signaling pathway in the context of the migration of these cells. One exception is AA861, an inhibitor of 5-lipoxygenase (5-LO). AA861 inhibited the EGF-induced migration of A431 cells and EC109 cells, but not EC17-CM-induced migration. Therefore, production of leukotriene(s) catalyzed by 5-lipoxygenase is required for EGF-induced cell migration, whereas EC17-CM may already contain leukotriene(s), so EC17-CM-induced cell migration was not inhibited by inhibition of 5-LO. In addition, a specific inhibitor of EGF-receptor tyrosine kinase (AG1478) potently inhibited the EC17-CM-induced migration of A431 and EC109 cells, but weakly inhibited migration of EC17 cells, indicating that EC17 cells might produce and secrete EGF, whereas EC17 cells underwent cell migration in response to migration factors other than EGF.

Interestingly, the mode of EGF-induced cell migration based on cell morphology can also be classified into clusters B and C. As shown in **Figure 1b**, A431 cells and EC109 cells in cluster B showed collective migration, whereas TT, TE8 and EC17 cells in cluster C showed a mesenchymal migration. With respect to collective migration, cells moved in groups and a leading cell at the tip of the group generated the migratory traction and the cells in the middle and at the back of the group were predominantly dragged passively. In contrast, mesenchymal migration required the formation of protrusions at the leading edge and actomyosin-mediated retraction of the trailing edge. This raises the possibility that the difference in the mode of cell migration of epithelial cells might be correlated with the differences in sensitivity to chemical inhibitors between clusters B and C. The ROCK inhibitor, Y27632, is a representative example; it inhibited mesenchymal migration of TT cells and TE8 cells more potently than collective migration of A431 and EC109 cells. Indeed, Rho-ROCK signaling is proposed to induce actomyosin-mediated retraction at the trailing edge in mesenchymal migration[15]. As an exception, the ROCK inhibitor Y27632 failed to inhibit mesenchymal migration of EC17 cells. At present, although we do not know why inhibition of ROCK did not suppress the migration of EC17 cells, one possible explanation is that another Rho effector, citron kinase or mDia, could regulate mesenchymal migration if used instead of ROCK. Moreover, the GSK-3 inhibitor (SB415286) and the p38MAPK inhibitors (PD169316 and SB203580) also inhibited the EGF-induced migration of TE8, TT, and EC17 cells more potently than they did in A431 and EC109 cells. This indicates that GSK3 and p38MAPK might be involved in the Rho-ROCK signaling responsible for mesenchymal migration. These ideas can be supported by other findings. GSK-3 phosphorylated and inactivated p190A RhoGAP, which is a key Rho regulatory protein in the context of cell migration. This resulted in the activation of Rho-ROCK signaling[31]. Furthermore, the phosphorylation of protein substrates by GSK–3 often requires the "priming" of a neighboring residue by a distinct kinase, leading to subsequent phosphorylation by GSK-3[32]. p38MAPK could effectively prime the C-terminal fragment of p190A RhoGAP for subsequent phosphorylation by GSK-3. The Chk1 inhibitor SB218078 also inhibited EGF-induced migration of TE8, TT, and EC17 cells more potently than it did in A431 and EC109 cells. However, at present we do not know how chk1 is involved in mesenchymal migration. Moreover, we cannot exclude the possibility that chk1 is important in mechanisms other than the mode of cell migration. Contrastingly, although PI3K, PP2A and HMG-CoA reductase somewhat selectively inhibited EGF-induced collective migration, the role of these enzymes on cell migration remains unclear.

In summary, we have shown that JNK is a signaling molecule common to all types of cell migration, and many molecules have diverse functions in the migration of particular types of cancer cells. We determined this using a chemical genomic approach. Our approach can be used as a tool for understanding the diversity and similarities in cancer cell migration signaling, opening up the potential for revealing novel molecular targets in cancer therapy.

Methods

Cell culture. 3Y1 and HT1080 cells were maintained in Dulbecco's Eagle's medium (DMEM) supplemented with 10% fetal bovine serum (FBS), 0.1 g/l kanamycin, 100 units/ml penicillin G, 0.6 g/l L-glutamine, and 2.5 g/l $NaHCO_3$. A431 cells were maintained in DMEM supplemented with 5% calf serum (CS), 0.1 g/l kanamycin, 100 units/ml penicillin G, 0.6 g/l L-glutamine, and 2.5 g/l $NaHCO_3$. B16 cells were maintained in DMEM supplemented with 8% FBS, 0.1 g/l kanamycin, 100 units/ml penicillin G, 0.6 g/l L-glutamine, and 2.5 g/l $NaHCO_3$. EC17, EC109, TE8, and TT cells were maintained in Roswell Park Memorial Institute (RPMI) medium 1640 supplemented with 5% FBS, 0.1 g/l kanamycin, 100 units/ml penicillin G, 0.6 g/l L-glutamine, and 2.5 g/l $NaHCO_3$. For routine culture, cells were incubated in a standard humidified incubator at 37°C in 5% CO_2.

Reagents. A23187, AG1478, ALLN, cytochalasin D, okadaic acid, rapamycin, and Y27632 were purchased from Calbiochem. MK571 was purchased from Cayman. Thapsigargin was purchased from Santa Cruz Biotechnology. AA861, bafilomycin A, LY294002, mevastatin, MG132, MK886, PD169316, SB203580, SB218078, SB415286, SP600125, tunicamycin, U0126, wortmannin, and epidermal growth factor were purchased from Sigma. Paclitaxel, radicicol, and vinblastine were purchased from Wako Pure Chemical Industries, Ltd. Herbimycin A, moverastin, and xanthohumol was purified from cultures of *Streptomyces sp.* in our own laboratory. Leptomycin B

and trichostatin A were kind gifts from Dr. Minoru Yoshida at RIKEN. Compound UTKO1 was synthesized and kindly donated by Dr. Hidenori Watanabe of the University of Tokyo. Alendronate and risedronate were kind gifts from Yamanouchi Pharmaceutical Co., Ltd (Astellas Pharma Inc.).

Preparation of conditioned medium (CM) from EC17 cells. EC17 cells (1.0×10^6 cells) were seeded in ϕ 100 mm dish. The following day, the medium was replaced with 10 ml of RPMI 1640 containing 1% FBS. After 24 h, the medium was recovered and sterilized by filtration.

Wound healing assay. A confluent monolayer of cells in a 48-well plate was scratched with a micropipette tip to create a cell-free zone in each well, about 1 mm in width. The medium was replaced with RPMI1640 with 1% FBS with or without test compound, and cells were either treated with the migratory stimulus or not treated with it so as to serve as controls. After a fixed period of time, cells were observed and photographed under a microscope. The experimental conditions for each cell line are described as Table 1. Wound areas were quantified using ImageJ software. After photographing, cells were trypsinized and collected, and cell viability was determined by trypan blue dye exclusion assay. Average migration inhibition scores were calculated from two independent experiments.

Cluster analysis. The value of migration inhibition was ordered according to the experimental conditions of cell migration or the compounds used. These profiles were analyzed by hierarchical clustering (using the method of Ward's linkage based on Euclidean distance) and visualized using a heat map using the R Project package (http://www.R-project.org).

1. Marshall, C. J. Ras effectors. *Curr. Opin. Cell Biol.* **8**, 197–204 (1996).
2. Klemke, R. L. *et al.* Regulation of cell motility by mitogen-activated protein kinase. *J. Cell Biol.* **137**, 481–492 (1997).
3. Nguyen, D. H. *et al.* Myosin light chain kinase functions downstream of Ras/ERK to promote migration of urokinase-type plasminogen activator-stimulated cells in an integrin-selective manner. *J. Cell Biol.* **146**, 149–164 (1999).
4. Tanimura, S. *et al.* Prolonged nuclear retention of activated extracellular signal-regulated kinase 1/2 is required for hepatocyte growth factor-induced cell motility. *J. Biol. Chem.* **277**, 28256–28264 (2002).
5. Keely, P. J., Westwick, J. K., Whitehead, I. P., Der, C. J. & Parise, L. V. Cdc42 and Rac1 induce integrin-mediated cell motility and invasiveness through PI(3)K. *Nature* **390**, 632–636 (1997).
6. Gan, Y. *et al.* Differential roles of ERK and Akt pathways in regulation of EGFR-mediated signaling and motility in prostate cancer cells. *Oncogene* **29**, 4947–4958 (2010).
7. Huang, C., Rajfur, Z., Borchers, C., Schaller, M. D. & Jacobson, K. JNK phosphorylates paxillin and regulates cell migration. *Nature* **424**, 219–223 (2003).
8. Wagner, E. F. & Nebreda, A. R. Signal integration by JNK and p38 MAPK pathways in cancer development. *Nat. Rev. Cancer* **9**, 537–549 (2009).
9. Narumiya, S., Ishizaki, T. & Watanabe, N. Rho effectors and reorganization of actin cytoskeleton. *FEBS Lett.* **410**, 68–72 (1997).
10. Nobes, C. D. & Hall, A. Rho, rac, and cdc42 GTPases regulate the assembly of multimolecular focal complexes associated with actin stress fibers, lamellipodia, and filopodia. *Cell* **81**, 53–62 (1995).
11. Etienne-Manneville, S. & Hall, A. Rho GTPases in cell biology. *Nature* **420**, 629–635 (2002).
12. Makrodouli, E. *et al.* BRAF and RAS oncogenes regulate Rho GTPase pathways to mediate migration and invasion properties in human colon cancer cells: a comparative study. *Mol. Cancer* **10**, 118 (2011).
13. Yarrow, J. C., Totsukawa, G., Charras, G. T. & Mitchison, T. J. Screening for cell migration inhibitors via automated microscopy reveals a Rho-kinase inhibitor. *Chem. Biol.* **12**, 385–395 (2005).
14. Kakinuma, N., Roy, B. C., Zhu, Y., Wang, Y. & Kiyama, R. Kank regulates Rho A-dependent formation of actin stress fibers and cell migration via 14-3-3 in PI3K-Akt signaling. *J. Cell Biol.* **181**, 537–549 (2008).
15. Sanz-Moreno, V. *et al.* Rac activation and inactivation control plasticity of tumor cell movement. *Cell* **135**, 510–523 (2008).
16. Kurokawa, K. *et al.* Coactivation of Rac1 and Cdc42 at lamellipodia and membrane ruffles induced by epidermal growth factor. *Mol. Biol. Cell* **15**, 1003–1010 (2004).
17. Scherf, U. *et al.* A gene expression database for the molecular pharmacology of cancer. *Nat. Genet.* **24**, 236–244 (2000).
18. Nakatsu, N. *et al.* Chemosensitivity profile of cancer cell lines and identification of genes determining chemosensitivity by an integrated bioinformatical approach using cDNA arrays. *Mol. Cancer Ther.* **4**, 399–412 (2005).
19. Muroi, M. *et al.* Application of proteomic profiling based on 2D-DIGE for classification of compounds according to the mechanism of action. *Chem. Biol.* **17**, 460–470 (2010).
20. Takemoto, Y. *et al.* Chemistry and biology of moverastins, inhibitors of cancer cell migration, produced by *Aspergillus*. *Chem. Biol.* **12**, 1337–1347 (2005).
21. Sawada, M. *et al.* Synthesis and anti-migrative evaluation of moverastin derivatives. *Bioorg. Med. Chem. Lett.* **21**, 1385–1389 (2011).
22. Kobayashi, H. *et al.* Involvement of 14-3-3 proteins in the second epidermal growth factor-induced wave of Rac1 activation in the process of cell migration. *J. Biol. Chem.* **286**, 39259–39268 (2011).
23. Sasazawa, Y. *et al.* Xanthohumol impairs autophagosome maturation through direct inhibition of valosin-containing protein. *ACS Chem. Biol.* (2012). doi:10.1021/cb200492h
24. Werno, C., Zhou, J. & Brüne, B. A23187, ionomycin and thapsigargin upregulate mRNA of HIF-1alpha via endoplasmic reticulum stress rather than a rise in intracellular calcium. *J. Cell Physiol.* **215**, 708–714 (2008).
25. Yamazaki, M., Chiba, K. & Yoshikawa, C. Genipin suppresses A23187-induced cytotoxicity in neuro2a cells. *Biol. Pharm. Bull.* **32**, 1043–1046 (2009).
26. Huang, C., Jacobson, K. & Schaller, M. D. A role for JNK-paxillin signaling in cell migration. *Cell Cycle* **3**, 4–6 (2004).
27. Sun, Y., Yang, T. & Xu, Z. The JNK pathway and neuronal migration. *J. Genet. Genomics* **34**, 957–965 (2007).
28. Ching, Y. P. *et al.* P21-activated protein kinase is overexpressed in hepatocellular carcinoma and enhances cancer metastasis involving c-Jun NH2-terminal kinase activation and paxillin phosphorylation. *Cancer Res.* **67**, 3601–3608 (2007).
29. Wang, J. *et al.* Sustained c-Jun-NH2-kinase activity promotes epithelial-mesenchymal transition, invasion, and survival of breast cancer cells by regulating extracellular signal-regulated kinase activation. *Mol. Cancer Res.* **8**, 266–277 (2010).
30. Pollard, T. D. & Borisy, G. G. Cellular motility driven by assembly and disassembly of actin filaments. *Cell* **112**, 453–465 (2003).
31. Jiang, W. *et al.* p190A RhoGAP is a glycogen synthase kinase-3-beta substrate required for polarized cell migration. *J. Biol. Chem.* **283**, 20978–20988 (2008).
32. Harwood, A. J. Signal transduction in development: holding the key. *Dev. Cell.* **2**, 384–385 (2002).
33. Abbott, B. J. *et al.* Microbial transformation of A23187, a divalent cation ionophore antibiotic. *Antimicrob. Agents Chemother.* **16**, 808–812 (1979).
34. Yoshimoto, T. *et al.* 2,3,5-Trimethyl-6-(12-hydroxy-5,10-dodecadiynyl)-1,4-benzoquinone (AA861), a selective inhibitor of the 5-lipoxygenase reaction and the biosynthesis of slow-reacting substance of anaphylaxis. *Biochim. Biophys. Acta.* **713**, 470–473 (1982).
35. Osherov, N. & Levitzki, A. Epidermal-growth-factor-dependent activation of the src-family kinases. *Eur. J. Biochem.* **225**, 1047–1053 (1994).
36. van Beek, E., Pieterman, E., Cohen, L., Löwik, C. & Papapoulos, S. Farnesyl pyrophosphate synthase is the molecular target of nitrogen-containing bisphosphonates. *Biochem. Biophys. Res. Commun.* **264**, 108–111 (1999).
37. Inoue, S., Bar-Nun, S., Roitelman, J. & Simoni, R. D. Inhibition of degradation of 3-hydroxy-3-methylglutaryl-coenzyme A reductase in vivo by cysteine protease inhibitors. *J. Biol. Chem.* **266**, 13311–13317 (1991).
38. Bowman, E. J., Siebers, A. & Altendorf, K. Bafilomycins: a class of inhibitors of membrane ATPases from microorganisms, animal cells, and plant cells. *Proc. Natl. Acad. Sci. USA* **85**, 7972–7976 (1988).
39. Cooper, J. A. Effects of cytochalasin and phalloidin on actin. *J. Cell Biol.* **105**, 1473–1478 (1987).
40. Whitesell, L., Mimnaugh, E. G., De Costa, B., Myers, C. E. & Neckers, L. M. Inhibition of heat shock protein HSP90-pp60v-src heteroprotein complex formation by benzoquinone ansamycins: essential role for stress proteins in oncogenic transformation. *Proc. Natl. Acad. Sci. USA* **91**, 8324–8328 (1994).
41. Nishi, K. *et al.* Leptomycin B targets a regulatory cascade of crm1, a fission yeast nuclear protein, involved in control of higher order chromosome structure and gene expression. *J. Biol. Chem.* **269**, 6320–6324 (1994).
42. Vlahos, C. J., Matter, W. F., Hui, K. Y. & Brown, R. F. A specific inhibitor of phosphatidylinositol 3-kinase, 2-(4-morpholinyl)-8-phenyl-4H-1-benzopyran-4-one (LY294002). *J. Biol. Chem.* **269**, 5241–5248 (1994).
43. Endo, A., Kuroda, M. & Tanzawa, K. Competitive inhibition of 3-hydroxy-3-methylglutaryl coenzyme A reductase by ML-236A and ML-236B fungal metabolites, having hypocholesterolemic activity. *FEBS Lett.* **72**, 323–326 (1976).
44. Lee, D. H. & Goldberg, A. L. Proteasome inhibitors: valuable new tools for cell biologists. *Trends Cell Biol.* **8**, 397–403 (1998).
45. Woszczek, G. *et al.* Functional characterization of human cysteinyl leukotriene 1 receptor gene structure. *J. Immunol.* **175**, 5152–5159 (2005).
46. Ford-Hutchinson, A. W. FLAP: a novel drug target for inhibiting the synthesis of leukotrienes. *Trends Pharmacol. Sci.* **12**, 68–70 (1991).
47. Bialojan, C. & Takai, A. Inhibitory effect of a marine-sponge toxin, okadaic acid, on protein phosphatases. Specificity and kinetics. *Biochem. J.* **256**, 283–290 (1988).
48. Schiff, P. B. & Horwitz, S. B. Taxol stabilizes microtubules in mouse fibroblast cells. *Proc. Natl. Acad. Sci. USA* **77**, 1561–1565 (1980).
49. Kummer, J. L., Rao, P. K. & Heidenreich, K. A. Apoptosis induced by withdrawal of trophic factors is mediated by p38 mitogen-activated protein kinase. *J. Biol. Chem.* **272**, 20490–20494 (1997).
50. Schulte, T. W. *et al.* Antibiotic radicicol binds to the N-terminal domain of Hsp90 and shares important biologic activities with geldanamycin. *Cell Stress Chaperones* **3**, 100–108 (1998).
51. Brown, E. J. *et al.* A mammalian protein targeted by G1-arresting rapamycin-receptor complex. *Nature* **369**, 756–758 (1994).
52. Gould, G. W., Cuenda, A., Thomson, F. J. & Cohen, P. The activation of distinct mitogen-activated protein kinase cascades is required for the stimulation of

2-deoxyglucose uptake by interleukin-1 and insulin-like growth factor-1 in KB cells. *Biochem. J.* **311** (Pt 3), 735–738 (1995).
53. Zhao, B. *et al.* Structural basis for Chk1 inhibition by UCN-01. *J. Biol. Chem.* **277**, 46609–46615 (2002).
54. Coghlan, M. P. *et al.* Selective small molecule inhibitors of glycogen synthase kinase-3 modulate glycogen metabolism and gene transcription. *Chem. Biol.* **7**, 793–803 (2000).
55. Han, Z. *et al.* c-Jun N-terminal kinase is required for metalloproteinase expression and joint destruction in inflammatory arthritis. *J. Clin. Invest.* **108**, 73–81 (2001).
56. Thastrup, O., Foder, B. & Scharff, O. The calcium mobilizing tumor promoting agent, thapsigargin elevates the platelet cytoplasmic free calcium concentration to a higher steady state level. A possible mechanism of action for the tumor promotion. *Biochem. Biophys. Res. Commun.* **142**, 654–660 (1987).
57. Yoshida, M., Kijima, M., Akita, M. & Beppu, T. Potent and specific inhibition of mammalian histone deacetylase both in vivo and in vitro by trichostatin A. *J. Biol. Chem.* **265**, 17174–17179 (1990).
58. Takatsuki, A., Arima, K. & Tamura, G. Tunicamycin, a new antibiotic. I. Isolation and characterization of tunicamycin. *J. Antibiot.* **24**, 215–223 (1971).
59. DeSilva, D. R. *et al.* Inhibition of mitogen-activated protein kinase kinase blocks T cell proliferation but does not induce or prevent anergy. *J. Immunol.* **160**, 4175–4181 (1998).
60. Owellen, R. J., Owens, A. H. & Donigian, D. W. The binding of vincristine, vinblastine and colchicine to tubulin. *Biochem. Biophys. Res. Commun.* **47**, 685–691 (1972).
61. Arcaro, A. & Wymann, M. P. Wortmannin is a potent phosphatidylinositol 3-kinase inhibitor: the role of phosphatidylinositol 3,4,5-trisphosphate in neutrophil responses. *Biochem. J.* **296** (Pt 2), 297–301 (1993).
62. Uehata, M. *et al.* Calcium sensitization of smooth muscle mediated by a Rho-associated protein kinase in hypertension. *Nature* **389**, 990–994 (1997).

Acknowledgements

We would like to thank Dr. M. Yoshida (RIKEN) for his kind gift of leptomycin B and trichostatin A; Dr. H. Watanabe (University of Tokyo) for his gracious gift of UTKO1; Dr. A. Funahashi (Keio University) for kind advice regarding data analysis. This work was supported by a Grant-in-Aid for Challenging Exploratory Research and JSPS Fellows, the Ministry of Education, Culture, Sports, Science, and Technology, Japan.

Author contributions

M.I. is responsible for project planning and experimental design; S.M. performed all of the experiments and statistical analyses; S.M., E.T. and M.I. co-wrote the paper.

Additional information

Competing financial interests: The authors declare no competing financial interests.

How to cite this article: Magi, S., Tashiro, E. & Imoto, M. A chemical genomic study identifying diversity in cell migration signaling in cancer cells. *Sci. Rep.* **2**, 823; DOI:10.1038/srep00823 (2012).

Kobayashi et al. BMC Chemical Biology 2012, 12:2
http://www.biomedcentral.com/1472-6769/12/2

BMC Chemical Biology

METHODOLOGY ARTICLE Open Access

Comprehensive predictions of target proteins based on protein-chemical interaction using virtual screening and experimental verifications

Hiroki Kobayashi[1†], Hiroko Harada[1†], Masaomi Nakamura[1], Yushi Futamura[1], Akihiro Ito[2], Minoru Yoshida[2], Shun-ichiro Iemura[3], Kazuo Shin-ya[3], Takayuki Doi[4], Takashi Takahashi[5], Tohru Natsume[3], Masaya Imoto[1] and Yasubumi Sakakibara[1*]

Abstract

Background: Identification of the target proteins of bioactive compounds is critical for elucidating the mode of action; however, target identification has been difficult in general, mostly due to the low sensitivity of detection using affinity chromatography followed by CBB staining and MS/MS analysis.

Results: We applied our protocol of predicting target proteins combining *in silico* screening and experimental verification for incednine, which inhibits the anti-apoptotic function of Bcl-xL by an unknown mechanism. One hundred eighty-two target protein candidates were computationally predicted to bind to incednine by the statistical prediction method, and the predictions were verified by *in vitro* binding of incednine to seven proteins, whose expression can be confirmed in our cell system.
As a result, 40% accuracy of the computational predictions was achieved successfully, and we newly found 3 incednine-binding proteins.

Conclusions: This study revealed that our proposed protocol of predicting target protein combining *in silico* screening and experimental verification is useful, and provides new insight into a strategy for identifying target proteins of small molecules.

Background

To understand complex cell systems, functional analysis of proteins has become the main focus of growing research fields of biology in the post-genome era; however, the roles of many proteins in cellular events remain to be elucidated. Among various methods to elucidate protein functions, the approach of chemical genetics is notable, with small molecular compounds used as probes to elucidate protein functions within signal pathways [1,2]. Indeed, several bioactive compounds have led to breakthroughs in understanding the functional roles of proteins [3-11]; however, one significant hurdle to developing new chemical probes of biological systems is identifying the target proteins of bioactive compounds, discovered using cell-based small-molecule screening.

A variety of methods and technologies for identifying target proteins have been reported [12]. Among them, affinity chromatography is often used for identifying biological targets of multiple small molecules of interest; however, it is usually very difficult to identify compound-targeted protein with low expression because of the low sensitivity of detection using coomassie brilliant blue (CBB) staining and MS/MS analysis. Thus, target identification of small molecules using affinity chromatography is severely limited. To overcome the limitations of affinity chromatography, we propose a new protocol combining *in silico* screening and experimental verification for identification of target proteins.

In our previous work, we developed an *in-silico* screening system, called "COPICAT" (Comprehensive Predictor of Interactions between Chemical compounds And Target proteins), to predict the comprehensive

* Correspondence: yasu@bio.keio.ac.jp
†Equal contributors
[1]Department of Biosciences and Informatics, Faculty of Science and Technology, Keio University, 3-14-1 Hiyoshi, Kohoku-ku, Yokohama 223-8522, Japan
Full list of author information is available at the end of the article

interaction between small molecules and target proteins [13]. If a target protein is input in the system, a list of chemical compounds which are likely to interact with the protein is predicted. In our previous work, several potential ligands for the androgen receptor were predicted by this system, these predictions were experimentally verified, and a novel antagonist was found [14]. On the other hand, if a chemical compound is input in the system, a list of proteins which are likely to interact with the compound is predicted by the system.

Previously, we isolated the natural product incednine from the fermentation broth of *Streptomyces* sp. ML694-90F3, which consists of a novel skeletal structure, enol-ether amide in the 24-membered macrolactam core, with two aminosugars. In addition, it was reported that incednine induced apoptosis in Bcl-xL-overexpressing human small cell lung carcinoma Ms-1 cells when combined with several anti-tumor drugs including adriamycin, camptothecin, cisplatin, inostamycin, taxol, and vinblastine [15]. Because this compound inhibits the anti-apoptotic function of Bcl-2/Bcl-xL without affecting its binding to pro-apoptotic Bcl-2 family proteins, it may target other proteins associated with the Bcl-2/Bcl-xL-regulated apoptotic pathway. To address the mode of action of incednine underlying its interesting function, we first synthesized affinity-tagged incednine which is biologically active (data not shown), and proteins bound to incednine were separated by SDS-PAGE followed by CBB staining, and each protein band was directly identified using liquid chromatography-tandem mass (LC-MS/MS) spectrometry analysis. Fifty-three proteins were identified as listed in Table 1, and some of which, such as eukaryotic initiation factor 4A3(eIF4A3), prolyl 4-hydroxylase, beta subunit (PDI), heat shock protein 70 (HSP70), and protein phosphatase 2A (PP2A) were reported to relate to cancer cell survival[16-19]. Therefore these were knocked down by siRNA or inhibited by a specific inhibitor, and assessed for their ability to modulate Bcl-2/Bcl-xL anti-apoptotic function, as does incednine. However, the candidate proteins tested did not appear to be the target responsible for modulating Bcl-2/Bcl-xL anti-apoptotic function (Additional file 1). Therefore, the target protein of incednine responsible for modulating Bcl-2/Bcl-xL anti-apoptotic function has not yet been determined, and further candidate proteins as targets of incednine are expected to emerge.

In this context, we propose a new protocol combining *in silico* screening and experimental verification for the identification of target proteins. We first predicted the candidate proteins likely binding to the input compound by applying the COPICAT system, and then employed western blotting to detect the binding of predicted proteins to the input compound. This method solves the problem of the low sensitivity of the traditional method (as illustrated in Figure 1).

Results

Computational prediction of target proteins for incednine

We set the chemical compound "incednine" as the binding ligand, and candidate proteins for the targets of incednine were computationally predicted from the KEGG database by using the statistical prediction method for protein-chemical interaction. The training dataset of protein-chemical interactions to construct the SVM-based statistical learning model was collected from the approved DrugCards data in the DrugBank database [20], and 53 interactions with incednine obtained from our previous binding experiments using affinity chromatography (see Table 1 and Methods) because the prediction accuracy was increased when more training samples of protein-chemical interactions were given to the SVM-based statistical learning model. Among 24,245 human proteins in the KEGG repository, 182 proteins were newly predicted as positive, that is, to interact with incednine with high probability greater than the 0.5 threshold (the default threshold value).

Clustering of computationally predicted proteins

The 182 proteins that were computationally predicted to bind to incednine were clustered by the hierarchical clustering method using 199-dimentional feature vector that was used for encoding amino acid sequences to construct the SVM-based statistical learning model (See Methods section for the details). Note that the similarity based on this 199-dimentional feature vector is different from the sequence similarity, and this similarity measure based on the 199-dimentional vector was proven to work well for protein-chemical interaction predictions in our previous work [13]. For example, 5HTT and AR α-1A showed only about 10% sequence similarity although both were reported to interact with the MDMA drug and successfully predicted by our SVM-based statistical learning method. A cutoff threshold on the constructed clustering tree was determined so that the proteins were clustered into 11 clusters and each cluster had a statistically significant number of members. The proteins predicted to bind to incednine are listed in Additional file 2.

Experimental verification

Next, to examine whether incednine can bind to the proteins, an *in vitro* biotinylated incednine pull-down assay using the lysate of Bcl-xL expressing Ms-1 cells was performed. We tested 16 proteins as pilot experiments, which are selected from each cluster by one or two based on antibody availability. Negative candidates that were predicted not to bind to incednine were extracted for experimental verification. These proteins, positive candidates and negative candidates, are listed in Table 2. Among positive candidate proteins, 2 positive candidates PIK3CG and ACACA were found to bind to

Table 1 List of proteins identified to bind to incednine in our previous binding experiments

Protein	Uniprot ID	Kegg ID
poly 4- hydroxylase, beta submit	P07237	5034
N-acylaminoacyl peptide hydrolase	P13798	327
Heat shock protein 70	P08107	3303/3304
Protein Phosphatase A2	P67775	5515
Similar to DNA damage-binding protein 1	Q16531	1642
Deoxyhypusin synthase isoform alpha	P49366	1725
Methionine adenosyltransferse alpha/beta	P31153/Q00266/Q9NZL9	4144/4143/27430
4-alpha-glucanotransferse	P35573	178
Actin alpha 4	O43707	81
Eukaryotic Initiation factor 4A3	P38919	9775
Deoxycytidine kinase	P27707	1633
ATP synthase H+ transporting, mitochondrial F1complex, alpha	P25705	498
prohibitin	P35232	5245
proteasome alpha 7subuit	O14818	5688
proteasome(prosome,macropain) subunit alpha type 8	Q8TAA3	143471
centaurin,beta 2	Q15057	23527
heterogeneous nuclear ribonucleoprotein A/B	Q99729	3182
heterogeneous nuclear ribonucleoprotein K	P61978	3190
heterogeneous nuclear ribonucleoprotein D	Q14103	3184
heterogeneous nuclear ribonucleoprotein A2/B1	P22626	3181
heterogeneous nuclear ribonucleoprotein A1	P09651	3178
heterogeneous nuclear ribonucleoprotein M	P52272	4670
small nuclear ribonucleoprotein polypeptide D2 family	P62316	6633
mitochondrial riblosomal protein L2	Q5T653	51069
mitochondrial riblosomal protein L20	Q9BYC9	55052
mitochondrial riblosomal protein L3	Q6IBT2	11222
mitochondrial riblosomal protein L40	Q9NQ50	64976
mitochondrial riblosomal protein L46	B2RD75	26589
mitochondrial riblosomal protein L49	B2R4G6	740
mitochondrial riblosomal protein L1	A6NG03	65008
mitochondrial riblosomal protein L37	Q9BZE1	51253
small nuclear ribonucleoprotein-assosiated protein B and B'	P14678	6628
cAMP-dependent protein kinase, regulatory subunit alpha 1	P10644	5573
phosphoribosyl pyrophosphate synthetase-associated protein 1	B2R6M4	5635
peptidylprolyl isomerase-like 2	Q13356	23759
thymoprotein isoform beta, gamma	P42167	7112
fructose-bisphosphate aldolase A	P04075	226
brain creatine kinase	P12277	1152
enolase 1	P06733	2023
Ewing sarcoma breakpoint region 1	Q5THL0	2130
fusion(involved in t(12;16) in malignant liposarcoma)	Q6IBQ5	2521
GDP dissociation inhibitor 2	Q5SX88	2665
nucleosome assembly protein 1-like 1	P55209	4673
nucleosome assembly protein 1-like 4	Q99733	4676

Table 1 List of proteins identified to bind to incednine in our previous binding experiments *(Continued)*

phosphoglycerate dehydrogenase	O43175	26227
triosephosphate isomerase 1	P60174	7167
clathrin heavy chain 1	Q00610	1213
clathrin heavy poly peptide -like 1	P53675	8218
glutamyl-prolyl tRNA synthetase	P07814	2058
retinoblastoma binding protein 7	Q16576	5931
retinoblastoma binding protein 4	Q09028	5928
tripartite motif-containing 28 protein	Q13263	10155
high glucose-regulated protein 8	Q9Y5A9	51441

incednine, and 5 positive candidates DAPK1, PIK3C2B, PIP5K3, CHD4, GTF2IRD2 did not bind to incednine. Among negative candidate proteins, 2 negative candidates BECN1 and KIF5B did not bind to incednine, and 1 negative candidate PARP1 did bind to incednine (Figure 2). On the other hand, ITPR1, PARP14, PLCB1, KIF1A, KIF21B, and RGPD5, listed as positive candidates in Table 2, were not well expressed and were not detected in Bcl-xL-expressing Ms-1 cells; therefore, accuracy of 40% (4/10), sensitivity of 66.7% (2/3) and precision of 28.6% (2/7) were achieved.

Discussion

For target identification using affinity chromatography, conventional method requires multiple steps as follows; SDS-PAGE, CBB staining, excision of gel, destaining, reduction, trypsinization, and application to *LC-MS/MS system* (7 steps); these steps can be cumbersome, time-consuming and require expensive installation. Furthermore, CBB staining used in conventional method can detect proteins over nanogram order. In contrast, our proposed protocol for predicting target protein allows us to use western blotting to detect proteins in picogram order. Indeed, we found two incednine-binding proteins by this prediction. Additionally, we can enhance the precision of COPICAT by feeding back the experimental results to the system.

In this work, PIK3CG, PARP1, and ACACA were revealed to bind to incednine by applying our protocol to identify potential target proteins of chemical compounds. These proteins are potential targets of incednine because it has been reported that these proteins are related to cancer survival and drug resistance, as follows.

PI3KCG encodes p110 catalytic subunit isoform p110γ and heterodimerizes with regulatory subunit p101, composing class IB PI3K in the PI3K family [21,22]. Although PIK3CG and PIK3C2B are distant homologous

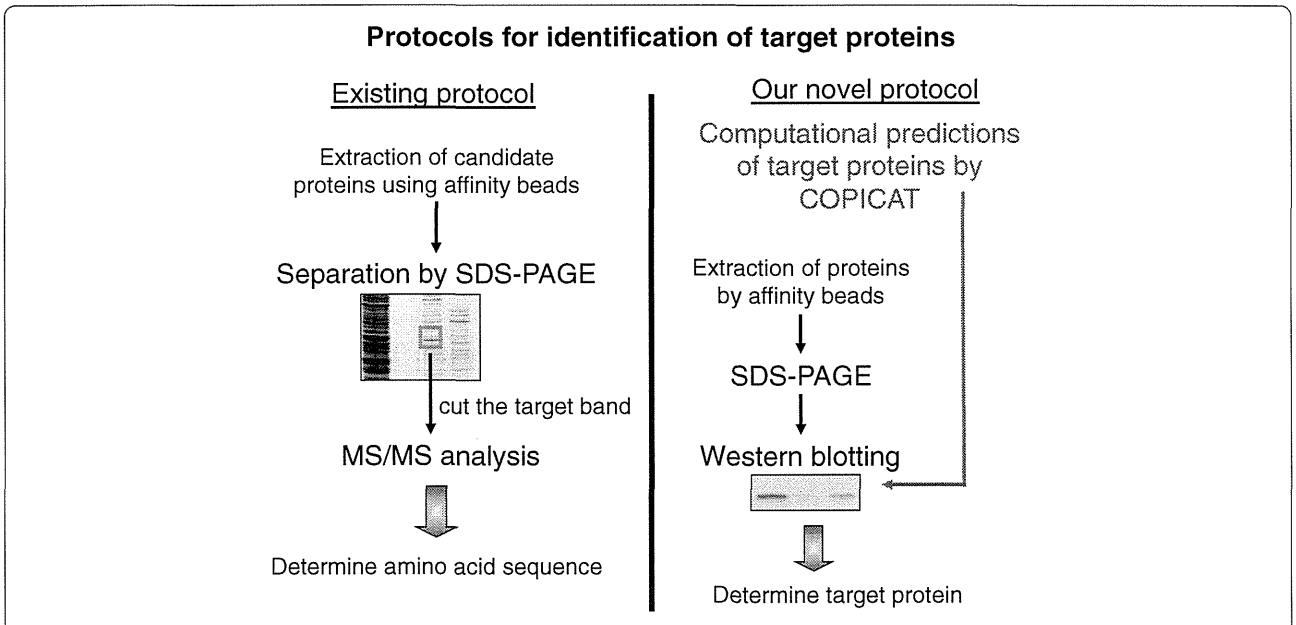

Figure 1 Schematic illustration of our protocol combining *in silico* screening and experimental verification for identification of target protein.